The University of Edinburgh
School of Engineering
Institute for Infrastructure and Environment
Academic Year 2014-2015

# Ignition of structures submitted to ember accumulation

Student: Simón Reinaldo Santamaría García

Promoter: Albert Simeoni

Master thesis submitted in the Erasmus Mundus Study Programme

**International Master of Science in Fire Safety Engineering**

**DISCLAIMER**

"This thesis is submitted in partial fulfillment of the requirements for the degree of The International Master of Science in Fire Safety Engineering (IMFSE). This thesis has never been submitted for any degree or examination to any other University/programme. The author(s) declare(s) that this thesis is original work except where stated. This declaration constitutes an assertion that full and accurate references and citations have been included for all material, directly included and indirectly contributing to the thesis. The author(s) gives (give) permission to make this master thesis available for consultation and to copy parts of this master thesis for personal use. In the case of any other use, the limitations of the copyright have to be respected, in particular with regard to the obligation to state expressly the source when quoting results from this master thesis. The thesis supervisor must be informed when data or results are used."

30 April 2015

Read and approved

## ABSTRACT

Wildland fires are a very complex phenomena that cause every year the loss of human lives as well as property damage and environmental concerns. This master thesis studies the phenomenon of wildfire spread to wooden structures in the Wildland Urban Interface (WUI). Focus is made on the analysis of ignition of wedges and corners due to the accumulation of hot embers during a fire. To study ember characteristics, data was collected from large scale experiments performed in the Pine Barrens, New Jersey, USA. It was found that most of the particles collected are slices of bark, and in a smaller quantity, branches and burned pinecones or pine needles, with an average mass per particle of less than 200 mg for more than 90% of them. To study the ignition of wood by conduction, small scale experiments were performed in the laboratory. Samples of Scottish redwood were exposed to different heating rates provided by an electrical heater. Thermal penetration on the wood is later compared to experiments using active heating (embers) on wood, active heating on an inert material and inert heating on an inert material. A comparison is made between the heat flux generated by embers and the heater and the effect on ignition.

# RESUMEN

Los incendios forestales causan cada año pérdidas de vidas humanas así como daños a la propiedad y consecuencias ambientales. Este trabajo de grado busca estudiar la propagación del fuego durante un incendio forestal hacia estructuras construidas en madera o materiales inflamables, en lo que es conocido como la interface entre la naturaleza salvaje y el desarrollo urbano (WUI, por sus siglas en ingles). El estudio está enfocado en los modos de ignición que se producen en geometrías específicas, como esquinas o uniones entre secciones. Para estudiar las características de las partículas calientes que aterrizan sobre dichas estructuras, se analizó la información recolectada durante una serie de experimentos a gran escala realizados en el estado de New Jersey, EEUU. Se encontró que la mayoría de las partículas provienen de la corteza de los arboles (los experimentos fueron realizados en bosques de pino); en menor cantidad fueron también recolectadas pequeñas ramas, así como otras piezas de la vegetación circundante. La masa promedio para más del 90% de las partículas es menor a 200 mg. Para estudiar la ignición de la madera debido a la exposición a un flujo de calor conductivo, se realizaron experimentos a pequeña escala en el laboratorio, usando un calentador eléctrico. La penetración térmica en la madera es estudiada en este reporte y los flujos de calor para diferentes condiciones experimentales (reemplazo del calentador por piezas de corteza o reemplazo de la madera por un material inerte) son comparados en un análisis final.

# INDEX

# LIST OF FIGURES

# LIST OF TABLES

# I. INTRODUCTION

Wildland fires are kwon to be very complex phenomena that affect human settlements trough the endangerment of human lives as well as public and private property. For many years, wildland fires (or wildfires) have been studied to try to understand their behavior and to reduce their probability of occurrence as well as their impact, once they have ignited.

The topic of wildfires has been studied by scientist from many different backgrounds and varied perspectives. Topics such as fire spread and fire intensity have coexisted in the research with fuel consumption and environmental impact. The topic is then one that fosters an increasing interest from the scientific community but it also entails a great deal of complexity for the analysts.

The Wildland Urban Interface could be defined as the area where human settlements encounter natural, uncontrolled or otherwise unrestricted vegetation. This term has been widely used in the literature to define those areas that are very much at risk during phenomena such as fires or floods. This thesis will focus on the Wildland Urban Interface (WUI), and the way fire spreads from wildland into wooden structures.

## 1.1 Problem Description.

As with any study of fire, the analysis process can be separated into ignition, fire behavior, fire spread and consequences of the fire. In wildfires, ignition can occur from many sources, some of them intentional (arson), some accidental (e.g. power lines that create sparks) and some can come from uncontrollable events (e.g. lightning).

Once a wildfire has been ignited, its development will depend on many factors, such as vegetation (fuel loading), environmental conditions, topography, suppression activities performed, etc. In this thesis, we will study the phenomenon of fire spread to human structures located close to the fire as a consequence of ember accumulation. Structures located in the WUI are exposed to ignition when a wildfire approaches. The ignition of wooden structures by radiation from the flames or from direct impingement of the plume has been widely studied (see 1.3 Literature Review). To avoid this, security perimeters have been defined to limit the minimum distance between the flame front and the structure.

However, when the fire goes through the vegetation, the buoyant force can lift and transport hot particles of wood, known as embers, which can land and accumulate on top of wooden or otherwise flammable structures and ignite the material. The phenomenon of flame spread due to hot embers is called spot ignition, although this term mainly refers to fire spread inside of the wildlands. It is necessary to study ember ignition since there is still much to be determined about the critical aspects that will lead to the ignition of structures.

## 1.2 Objectives.

This thesis has been structured to provide some insight into ignition of wooden wedges and corners submitted to ember accumulation. The idea is to gain a better understanding of the ignition phenomenon of houses or wooden structures that are submitted to showers of hot embers during a wildland fire.

To reach this objective, several goals have been proposed that define the structure, separation and design of the overall thesis. There are two main factors to be studied: the characteristics of the embers and the heat transfer between embers and the wood that lead to ignition. For this reason, the project is clearly divided into the two specific goals shown below:

1. Characterize embers collected from a large-scale, wildfire experiment: This will include an analysis on the collection protocol, the results, the possible sources of error and an interpretation on how this results could be linked with the second part of the project. Main aspects to be targeted for specific analysis are:
   - Density of firebrand collection.
   - Distribution of the firebrands depending on their origin (bark, branch, etc.).
   - Effect of fire behavior on fire brand generation.
   - Comparison of the results with similar experiments.

2. Perform small scale experiments to understand the ignition of wood wedges caused by ember accumulation. To do this, different experiments will be designed so that it is possible to separate the effect of the smouldering combustion of the embers on the heat transfer to the wood, taking into consideration the way wood reacts and decomposes at high temperatures. A big emphasis will be made on understanding the ignition of wood by conduction.

## 1.3 Literature Review.

Millions of acres and hundreds of structures are destroyed annually by wildfires [1]. [18] summarizes some experiences that have resulted in the losses of human lives and property damage due to wildfires in the past 15 years in Europe. In particular, the description of the Guadalajara wildfire (Spain, 2005) shows the impact of spotting and flame spread through firebrand generation. Several firefighters lost their lives in a situation where spot fires created around their position rendered their extinguishing efforts useless and prevented them from fleeing the area.

Wildfires have also been studied from different perspectives. In [17] the topic of wildfire is studied from both a safety and an ecological perspective. The traditional view on wildfire has been to prevent and extinguish it at all cost. However, [17] reports that "fire plays a vital role in the maintenance of the health of many ecosystems". This report of the USDA also provides a definition of the Wildland Urban Interface: "any area where humans and their development meet or intermix with wildland fuel".

Many studies have been performed on the phenomenon of ember ignition and fire spread due to spotting. The process is usually divided into three phenomena: Ember generation, transport and landing. Our issue of concern focuses on the landing of hot embers and the subsequent ignition process in the wooden structure. As will be done in the rest of the report, landing of embers and ignition of wood are going to be approached separately for clarity.

### 1.3.1 Embers

Ember generation and transport are not the main focus of this study but they are still considered since they provide an overall understanding of the problem In [1] the trajectory of embers lofted by ground fire plumes (surface fires) is studied. A model that considers the burning and wind carrying of embers and compares the trajectories for different geometries was developed. The results show that for embers with the same initial mass, disks propagate the farthest and have the highest remaining mass fraction upon impact on the ground. Cylinders have the smallest mass fraction upon impact. Although it is seen that charring embers travel slightly farther due to lower densities, the consideration on whether or not a particle is more dangerous in terms of spotting depends on the fragility of the reactions, which in turn leads to the conclusion that "a burning landing particle does not necessitate that it will ignite its surroundings". The paper shows the necessity for deeper studies on ignition by landing of hot embers.

[6] studied the ignition of forest litter by firebrands using samples of a manufactured material to simulate the embers, with especial consideration to the transition between smouldering and flaming ignition. It was clear that ignition probability has a high dependence on the moisture content of the fuel, and for a FMC higher than 10%, the effect of wind becomes more important. The effect of wind will not be considered in this report but it remains a critical variable in the ignition process.

[3] analyzes home ignitability during wildland fires. The analysis is based on data obtained from fires in the US and it quotes many different figures that bring into context the severity of the problem. The report focuses on the probability of ignition of houses in the WUI. Although a bigger focus is made on ignition by radiation from the flame or impingement of the plume, the importance of ignition of firebrands its highlighted trough the argument that roof flammability has a significant impact on the index of home survival. The concept of Flux Time Integral is used to account for the relevance of the effects of intensity of the fire and time of exposure.

In [4] experiments were performed to analyze the ignition of structures due to crown fires. The paper is based on results from the International Crown Fires Modelling Experiment (1195-2001). It focuses on studying ignition of wooden structures on the WUI due to radiation from the flame. Considering only radiation and making several assumptions (geometry, emissivity, residence time, etc.) a critical heat flux is calculated from a model and them compared to measurements on the field. The focus is made on flaming ignition, which is defined as a sudden temperature increase in the wood reaching 500°C.

[11] and [9] have studied the impact of firebrands into common construction configurations, most of them applicable to US standards. [9] evaluates current procedures and building standards through the use of a wind tunnel that is connected to a device (NIST Dragon) designed to imitate the continuous creation of firebrands at different burning states. The results were affected by many factors, such as material, angle of impact and ignition state of the firebrands. It is not clear how (or if) the results can be extrapolated to different materials and configurations. [10] uses a similar methodology to study the phenomenon of spotting and fire spread through the ignition of mulch and grass due to landing firebrands.

[7] studies spotting ignition for large scale experiments. Wind is mentioned to be the most critical factor for ignition; although all weather conditions play an important role. The difference between long-range and short-range firebrands is analyzed, considering lifetime of burning,

geometry, and driving forces. A very complete summary of previous experiments shows that must of the focus on research has been on understanding generation and transport of firebrands. It is concluded that although research on transport has advanced the understanding of the phenomenon, the current state of knowledge on generation of, and ignition by firebrands is insufficient to develop a predictive model. Finally, [7] states that the ignition of recipient fuels should be studied with a focus on two aspects: required energy for ignition of the recipient fuel and the amount of energy carried by a firebrand. Both aspects are touched upon in this report.

### 1.3.2 Ignition of wood.

[16] studied the influence of temperature, density, porosity and anisotropy on thermal conductivity and diffusivity of wood. It was found that, as expected, the thermal conductivity was higher at higher temperatures and that the conductivity decreases as the porosity of the material increases. Results showed that a temperature increase from 20 to 100 °C leads to an increase in conductivity of 14 to 24% in longitudinal and transverse directions. Heat transfer through the wood is not simple conduction, since the voids in the material are filled with air which also changes its density depending on the temperature of the sample. A model to determine thermal conductivity was created based on the ratio between conduction in parallel and serial layers of gas, liquid and solid phases.

[8] studied the material properties and the external factors that have the largest influence on the charring rate of wood. A study of the literature is made and results are compared. It was not possible to identify the factor with the highest influence since conditions between the tests vary. Five different zones during combustion of wood based on the temperature are defined: <100°C, 100-200°C, 200-280°C, 280-500°C, 500-1100°C; where a different phenomenon can be identified in each one of them. The summary shows that the rate of combustion is mainly governed by density, permeability along the grain, moisture ratio and thickness of char. External factors such as the thermal exposure/heat flux and the oxygen concentration also show large effects on the charring rate.

[2] performed an experimental and theoretical study of the ignition of wood, including convective effects. In many solid phase calculations, the solid is considered to be inert; however, evidence was found to invalidate this assumption since thermal decomposition of the wood occurred significantly before ignition. The degrading of the sample shows two consecutive stages: an endothermic one where decomposition of cellulose and part of hemicellulose take

place and a second, exothermic one where decomposition of lignin takes place. The study focuses on determining and comparing theoretical and experimental times to ignition (flaming) and smouldering. The results show good agreement between the two approaches.

[15] examines the ignition of wood samples in the cone calorimeter. A dual approach is used, where experiments are compared to a theoretical model. The ignition mechanism of wood was found to be different at lower heat fluxes than at higher heat fluxes. The difference is believed to be caused by char oxidation prior to flaming ignition. Temperature dependence of properties of wood (density, moisture content, thermal conductivity, specific heat and thermal inertia and diffusivity) is also studied. The theoretical model assumes the solid to be inert up to ignition. Ignition temperature by a radiant heat flux is determined (374°C) and compared to values in the literature. Good agreement is shown.

[14] uses a similar approach to [15]. The horizontal burning of four species of wood exposed to different heat fluxes is analyzed and a one-dimensional integral model is created. The model describes the transient pyrolysis of a semi-infinite charring solid subject to a constant heat flux. The model is thoroughly described and then the results are compared with the experiments, using analytical short-term and long-term solutions. Burning rate, thermal penetration and char depth are predicted by the model. Results agree very well in short times ($t < 45$ min). For longer times, poor agreement could be due to the infinite thickness assumption made on the model (losses on the back surface).

# II. METHODOLOGY

As explained in the Introduction, the overall objective of this project is to analyze the spread of WUI fires by attempting to understand the process of ignition of wooden structures by falling embers. In accordance with this, the project has been clearly divided into two main aspects that will be separately studied:

1. Ember collection and analysis from large scale field experiments.
2. Heat transfer and ignition of wood in small scale laboratory experiments.

Results will be obtained and individually analyzed and then a connection will be made between the two aspects. The work done in this project for both items mentioned above has been completed in conjunction with another master thesis completed at The University of Edinburgh by Bs. Kamila Kempna. All data is being analyzed in parallel and both reports will be introduced by the end of April. Therefore, it will be common in this report to quote results and analysis made on that thesis since both projects are considered to be complementary and provide different insights into the understanding of the problem.

The first part derives from a bigger project completed by the USDA Forest Service, the New Jersey Forest Fire Service and The University of Edinburgh. The project is designed to study the behavior of a prescribed fire as well as to quantify and predict its impact on fuel load in the Pine Barrens Reserve, NJ, USA. For this project, three different prescribed burns where instrumented (March 2013, 2014 and 2015). Summaries of data obtained and conclusions have already been submitted regarding the experience of 2013 [12] and [5]. Data for the experiment performed in 2014 is currently being analyzed and some initial results are available for the 2015 experience.

During each of these fires, several instrumentation techniques were used to obtain data on fire behavior and its impact on the fuel load and weather conditions. According to [12], point measurements were made using a combination of 4 overstory towers (towers taller than the canopies of the trees), 12 understory towers and 3 Fire Behavior Packages (FBP). Fire Behavior Packages provided measurements of vertical and horizontal wind velocity, temperature at different heights and incident heat flux from the flame front.

In addition to this, aerial IR images were recorded using Rochester Institute of Technology's Wildfire Airborne Sensor Program (WASP) to obtain time-stamped and georeferenced images of the fire evolution. This data will not be thoroughly analyzed in this master thesis and it will only

be used to support some of the conclusions regarding the embers collected in all plots. Other papers will properly analyze the information obtained from this instruments.

Finally, three different ember collection plots were located to collect and characterize the embers generated by the fire. Our project will only focus on those embers collected in 2014 and will mention the protocol that was designed and used for the 2015 experiment, although results on this year will not be analyzed for reasons explained bellow. Results of 2014 will be compared with those obtained in 2013.

### 2.1 Ember collection on 2014

Three different ember plots were used to collect firebrands. Ember plot 1 (E1) and Ember plot 2 (E2) were located inside of the forest, in areas where the fire front was expected to reach very closely to the pans. Ember plot 3 (E3) was located in a fuel break, close to the fire boundaries but it was not directly impacted. Figure 2.1 shows a satellite picture of the terrain with the location of all instrument towers and ember collection plots.

20 pans per plot were used with an area of 0.07 $m^2$ per pan for a total area of 1.4 $m^2$. All pans were identified by number and measurements were taken by pan. However, analysis are made by plot and only in specific cases a difference is made between different pans on the same plot.

E1 and E2 are located close to instrumented towers (3 and 7 respectively) and E3 is located close to the overstory tower located outside of the fire perimeter. All ember plots are supported by a non-flammable board (gypsum board) lifted by wooden supports from the ground to reduce the collection of dirt.

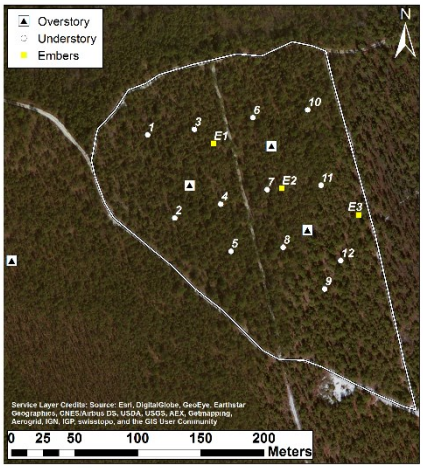


Figure 2.1. Satellite photograph of the parcel, indicating all overstory and understory tower as well as the location of E1, E2 and E3. Reproduced with permission.

In the aftermath of the 2014 experiments, manual measurements were taken with a caliper of the length, width, thickness and mass of each particle. They were also grouped into different categories depending on their origin (bark, branch, pinecone, needle, etc.). This work was carried out before this thesis was started and it proved to be a very time consuming endeavor. For this reason, only 41 out of the 60 pans were covered. During the 2015 experiments the content of the remaining 19 pans was measured and then all the data is analyzed. The precision of the caliper used to manually measure the embers is 0.01 mm. The precision of the weight scale is 0.01 mg.

There is, however, a big difference between the techniques used in 2014 and 2015 to measure the size of each particle. In 2015, to measure the area of every particle an algorithm was programed (further explained in research papers covering the 2015 experience) that detects the contrast in the picture between black (or dark grey) pixels and the white background. The software is then able to count all pixels and by using a reference length it can determine the total area of the particle. Figure 2.2 shows a sample of the pictures taken with the corresponding mass. The resolution of the software is $4.85*10^{-5}$ $m^2$.

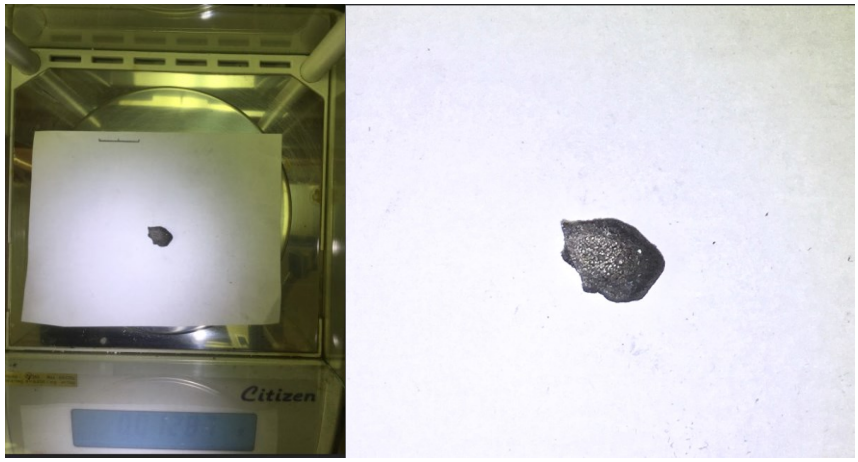


Figure 2.2. Right: original picture taken for Ember number 4, pan 10, ember plot 2. Left: picture after processing to be used by the software .E2 – 10 – 04.

Not all embers collected were measured. Embers too light (mass < 5 mg) were not considered individually, however, they were all group per pan and their total mass was recorded for further analysis.

## 2.2 Ember collection on 2015

In 2015, a third prescribed burn was completed in the same terrain as the one used in 2013. The idea was to quantify the effectiveness of prescribed fires on fire behavior. As in the years before, understory towers, overstory towers and Fire Behavior Packages (FBP) were used to obtain relevant data from the fire. The results have not been analyzed yet, but observations in the field showed a much less intense surface fire.

A similar set up for the ember collection plots was used. Mainly because of the low intensity of the fire, the fact that the bark on the trees had not fully recovered from the 2013 experiment (charred wood was a constant in all trees) and low wind velocities on the day of the burn, we did not collect any embers on this experiment. Therefore, there is no data (ember related) to analyze in this thesis.

However, the methodology used differed from the previous experiments and it is believed it will provide more accurate results. Appendix A.7 shows the summarized protocol for ember collection.

There are two problems associated with ember collection that were identified from the 2013 and 2014 experiments: extinguishing the particles as soon as they land and differentiating hot particles (capable of igniting structures) from cold particles that also land in the trays.

To avoid particles from burning further, the collecting pans were filled with water in 2013 and 2014. Although this does extinguish the embers, it creates two problems: first, there is no way to distinguish hot and cold embers falling on the tray and second, it is not possible to determine their position at landing. Another solution used in some, but not all of the pans, was to cover each pan with a thin foil that would be melted by hot particles (allowing them to land in the water) and would repel cold particles.

IR imaging of the landing particles showed that some hot particles that landed on the foil were lifted, almost immediately, by the wind and were not being collected. Also, in some pans the foil collapsed after it was perforated several times by different embers.

The 2015 methodology had then the objective to use a different solution that will permit the collection of particles ensuring that: first, a separation between hot and cold landing particles could be made and second, that burning particles will be extinguished a few seconds after landing.

Previous investigation led to the choice of an extinguishing gel called Protecto Forrest. The gel comes in a powder form and when mixed with water creates a solution that extinguishes the embers but also holds them in one place. To determine the temperature of the particle, irreversible Thermocronic ink was used. Thermocronic ink reacts to a change in temperature by changing its color (the ink that was used changed from a light pink to a dark purple when exposed to higher temperatures). The goal is to get a hot/cold distribution of embers from the solution with ink, and to get the individual mass of every ember from the solution with the extinguishing gel.

### 2.3 Heat transfer and ignition of wood in small scale laboratory experiments.

The second part of the project includes the small scale, laboratory experiments that are designed to understand the process of wood ignition by ember accumulation. The idea is to analyze the heat transfer that occurs between the embers and the wood by characterizing each phenomenon independently. With this in mind, four types of experiments were designed:

1. Analysis of the impact of inert heating on the wood (heater + wood).
    a. Heater aligned parallel to the grain (similar to real life, ember exposure situation).
    b. Heater aligned perpendicular to the grain.
2. Analysis of the impact of inert heating on an inert material (heater + vermiculite)
3. Analysis of the impact of embers on an inert material (embers + vermiculite)
4. Analysis of the impact of embers on wood (embers + wood // charcoal + wood).

In this project, specific results are shown for experiments of the types 1 and 2. Experiments for category 3 and 4 are analyzed in depth in Kamila Kempna's thesis, and the results are quoted in this project.

Figure 2.3 shows the schematics of the experimental set up for experiments category 1 and 2. The table shown is only half of the available set up for all the experiments. Two symmetric tables are available and they are designed in such a way that the distance between them and the angle that they form when joined together can be varied to study ignition behavior under different circumstances. The full table is used when completing type 3 or type 4 experiments. However, for the case of inert heating (heater), only half of the table, as is shown in Figure 2.3, is used.

The wood samples used for this tests were bought from a local supplier. They were described as Scottish Redwood with a thickness of 20 mm. Every sample has a width of 150 mm and a length of 260 mm. The graph on the right in figure 2.3 shows the experimental set up when the electrical heater is being used. All samples of wood were dried in an oven at a temperature of 100 ºC until their mass was constant.

The heater used is a strip electrical heater with a length of 13 cm and a width of 3.81 cm. It is designed for a standard supply of 120 V at which it provides a power of 150 W. In the experimental set up, a voltage variator was included to alter the electrical supply and this way analyze the influence of different heat fluxes. Throughout all the experiments, three different supplies were used: 60 V, 90 V and 120 V.

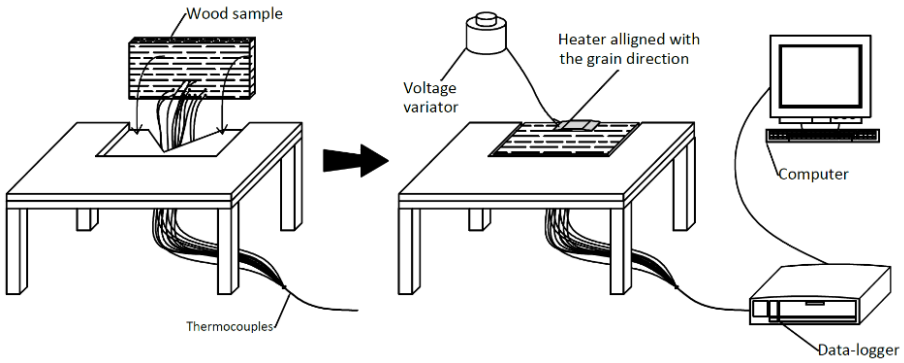


Figure 2.3. Experimental set up used for tests with the electrical heater.

Figure 2.4 shows the location of the thermocouples in the wood sample. All the thermocouples used are type K, with a beat diameter of 0.7 mm and a sheath diameter of 1.5 mm. The wholes for the thermocouples are 2.5 mm in diameter. For the final experiments (insulated samples + surface temperature), holes with a diameter of 2 mm were drilled and the thermocouples were fixed with aluminum tape, avoiding the flow of air into the thermocouple hole and also preventing the movement of the thermocouple inside of the sample.

All of the thermocouples are exposed, connected to a single data logger. 12 thermocouples were used for every experiment plus additional thermocouples in case the contact surface temperature (heater-wood) was being recorded. The figure also shows the coordinate system that was chosen. The x axis corresponds to heat transfer trough the wood, from the upper to the lower face. The y axis corresponds to heat transfer perpendicular to the grain and the z axis to heat transfer parallel to the grain. In these experiments (with the exception of experiments 13-15), the heater is aligned in the z direction.

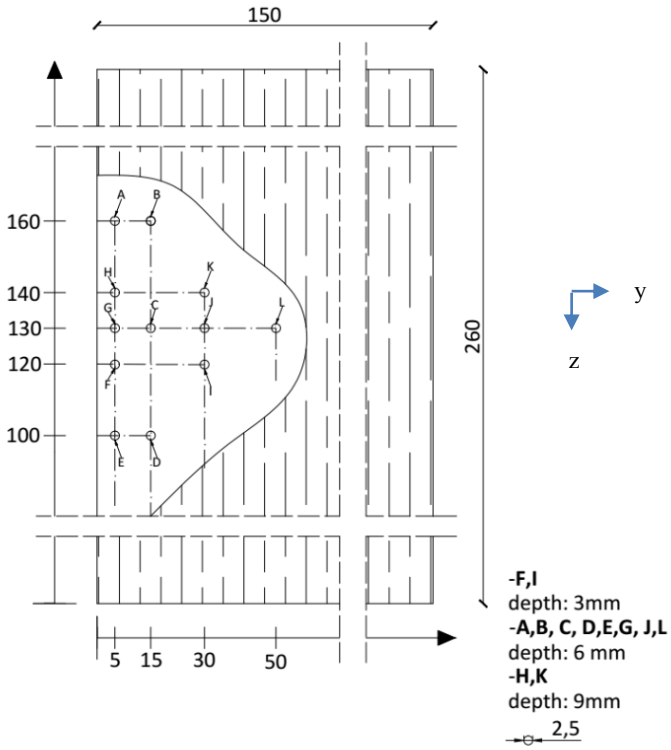


Figure 2.4. Distribution of thermocouples and axis convention. Location of thermocouples used for tests where the heater was placed parallel to the grain.

Figure 2.5 shows the location of the thermocouples for the additional study of conduction in wood with a perpendicularly aligned heater. Note that the disposition of the thermocouples remained the same but rotated 90°. In this sense, it is possible to analyze temperature values in the z axis and compare those to the values obtained for the temperature profile in the y axis in the previous experiments. Experiments will be conducted in three different sets: initial experiments for a qualitative analysis of the behavior, experiments with insulated wood and controlled heating time and experiments with insulated wood, controlled heating time and measurement of surface (contact) temperature.

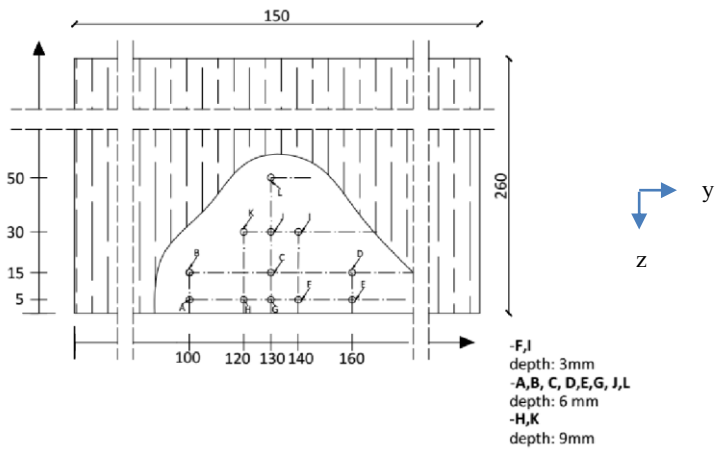


Figure 2.5. Distribution of thermocouples and axis convention. Location of thermocouples used for tests where the heater was placed perpendicular to the grain.

# III. RESULTS & DISCUSSION

## 3.1 Ember collection

As explained in the methodology, we will focus the analysis for the ember collection project on the results obtained in the 2014 experiments.

Figure 3.1 shows the way the different measured particles are distributed by plot. Mainly, embers collected were constituted by bark and branches. Pieces of burned pinecones and needles were also collected in lesser amounts and are grouped under the category "other". With the exception of plot 3 (which was located outside of the burning plot, on a fuel break), in ember plots 1 and 2, bark constitutes the majority of the particles collected.

In Figure 3.1 the percentage per plot is shown (over 80% is bark in plot 1, over 70% in plot 2 and over 30% in plot 3). However, arranged by mass, bark constitutes 79.14% of the mass in plot 1, 45.28 % of the mass in plot 2 and 34.53% of the total mass collected in ember plot 3. In contrast, "other" particles represent less than 5% of the mass in ember plots 1 and 2 and less than 15% of the mass in ember plot 3; for this reason our specific analysis will not cover them. The total mass collected by plot is 1114.1 mg in E1, 137953.51 mg in E2 and 322.31 mg in E3, providing final loads of 795.79 $mg/m^2$, 98538 $mg/m^2$ and 230.22 $mg/m^2$, respectively.

Figure 3.1 also shows the mass average for all the bark particles collected and the $75^{th}$ mass percentile value. As will be analyzed later, in ember plot 2 the number of particles collected (1458) represents a 1030% increase from the number of particles measured in plot 1 and a 3390% increase from those measured in plot 3. This is explained by two reasons: physical variables (such as fire behavior, location of the ember plot, wind conditions, etc.) resulted in more embers collected but also, the new measuring technique provided that much more particles were measured in this plot than would have otherwise been discarded, had the manual technique been used.

A different section will analyze the fire intensity and wind conditions close to each plot, but it can be noted that the big difference between the average value and the $75^{th}$ percentile for the bark mass in plot 2 is due to the collection of thick particles that are constituted by several slices of bark. Also, during the manual measurements for plots 1 and 3, some particles considered as "too small" where not individually measured but their overall mass and their quantity was

registered. In ember plot 2 the minimum size to measure a particle was lowered so more embers were taken into account.

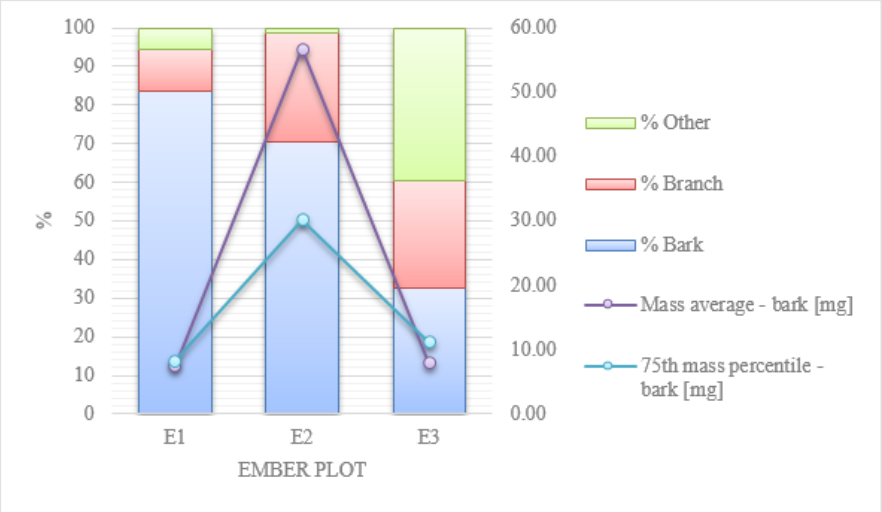


Figure 3.1. Distribution of particles collected in all ember plots (2014). Figure also shows mass average (mg) for bark particles in each plot and values for 75$^{th}$ mass percentile (mg).

### 3.1.1 Study of Bark. E1&E3.

The way bark particles were measured affects directly the results by modifying two main parameters: the area and the thickness. Each method provides a different accuracy for these quantities. The manual method used in plots 1 and 3 included an individual measurement of thickness for every particle, which means that it is possible to use this value to determine the density for each individual ember collected. Calculating the density is relevant since it provides an idea on the possible mass loss and relative remaining combustible energy in the embers. However, to determine the area, each particle's length and width was measured and then it was assumed that all particles have a rectangular surface, so the area was determined as width * length. This deviates from reality and can result in considerable errors.

At the moment this analysis was made, the embers collected in plots 1 and 3 had already been discarded. It is then not possible to re-measure this particles using the more accurate technique. One way of obtaining an idea of the possible errors associated to this is by comparing the maximum errors that could arise if different geometrical shapes (representing the different surfaces of bark) are assumed to have a rectangular area. For example, by assuming that a triangle (base = width measured and height = length) is a rectangle, there is an overestimation in

the area of 50%. In the case of a circle the value is closer to 52% (taken the diameter as the width). This is only a coarse estimation of how big the error can be, but it serves to create an idea on the impact of the rectangular shape assumption.

A qualitative analysis on the shape of embers measured in plot 2 resulted in a majority of the embers having similar shapes, making the assumption a logical one. There is no way to determine this with accuracy, but the method developed for plot 2 can be used in the future to obtain more accurate measurements.

If the area is overestimated the density calculated will be lower. The density of burn particles can be used to analyze how much did the embers burn during generation and transport (assuming they were extinguished at landing and that the initial density of bark samples is measured prior to the fire). Higher densities (than those calculated) for burnt and partially burnt particles means that when this data is used to determine likelihood of structural ignition by a shower of embers, particles with enough energy may be discarded.

The relation between the energy content of a particle at landing and the probability of ignition of a structure has not yet been determined, and it will depend on many external factors, including (but not limited to) the temperature of the ember and the characteristics of the material. However, if the pieces of bark shown were ignited and transported to the ember collection trays, we could say that a higher particle density could be an indicator of a higher energy content and by underestimating its value we would be underestimating the ignition potential. Hence, a precise measurement of the area is of the highest importance.

Table 3.1. Average thickness values for different surface areas. Ember plots 1 and 3. Range is defined in mm2 (0-100, 100-225, etc.) and thickness in mm.

| Range | # | % | Cumulative % | Average Thickness | Maximum Thickness | Minimum Thickness |
|---|---|---|---|---|---|---|
| 100 | 102 | 77.27 | 77.27 | 0.96 | 2.18 | 0.19 |
| 225 | 18 | 13.64 | 90.91 | 1.32 | 1.81 | 0.56 |
| 400 | 11 | 8.33 | 99.24 | 1.60 | 2.53 | 1.10 |
| 625 | 1 | 0.76 | 100.00 | 3.17 | 3.17 | 3.17 |

In table 3.1, the bark collected for plots 1 and 3 was sorted depending on its surface area. Four different area categories are defined for the 132 embers. The table shows the average, maximum and minimum thickness values for each category. The column range defines the interval (0-100,

100-225, 225-400 and 400-625). Table A.4 in Appendix A shows a similar analysis but without separating the bark embers by category. 90.7% of the pieces that were measured have a thickness between 0.5 mm and 2 mm. 97.73% of the embers have a thickness of 2 mm or less. This is in agreement with what was found in [5].

According to [5], in the 2013 experiments, the measurements of bark reduction of pine trees due to consumption during the fire was in the range of 0.32 to 4 mm, with a highest value of 14 mm. Bark reduction in the pine trees was measured directly by estimating the diameter of different trees located close to the FBP, before and after the fire. Thickness values of collected pieces of bark ranged between 1 and 6 mm. It is also highlighted by [5] that measurements could have been affected due to delamination or expansion of bark during the fire.

Figure 3.2 shows values of density for bark collected on plots 1 and 3. The graph on the left only shows values for embers with an area of 500 $mm^2$ or less (which represent 95% of bark collected). The figure in the graph shows scatter in the data for particles with an area of 100 $mm^2$ or less. It seems difficult to extract a pattern or clear behavior from the data shown below, but we can clearly see that the majority of particles show a density between 0.06 $mg/mm^3$ and 0.12 $mg/mm^3$. In 2013 [5] it was shown that the bark particles collected in the pans are related to intensity of the fire and can be associated to regression rates of the tree trunks, which in turn serve to understand the approach of collection of short-range particles and their dependence on fire characteristics.

There are two factors that directly affect the density analysis. The first one is the way the area is measured (as already covered). It is also worth mentioning that for smaller particles, the absolute error of the measurement remains the same (since the instrument does not change) but the effect increases as the size of the particle decreases, making the volume estimation a less accurate one. This also contributes to the scattering of the data in Figure 3.2 for small particles (Area < 100 $mm^2$). Another factor is the surface/volume ratio. This ratio has been assumed to be the same for all particles, therefore the mass loss of each piece of bark does not depend on the geometry. In reality, that is not the case. Different geometries will impact the overall burning behavior and ultimate mass loss. Particles with irregular geometries and more faces exposed to the fire will have higher surface/volume ratios (for similar volumes) and they will heat up and burn faster, lowering their density.

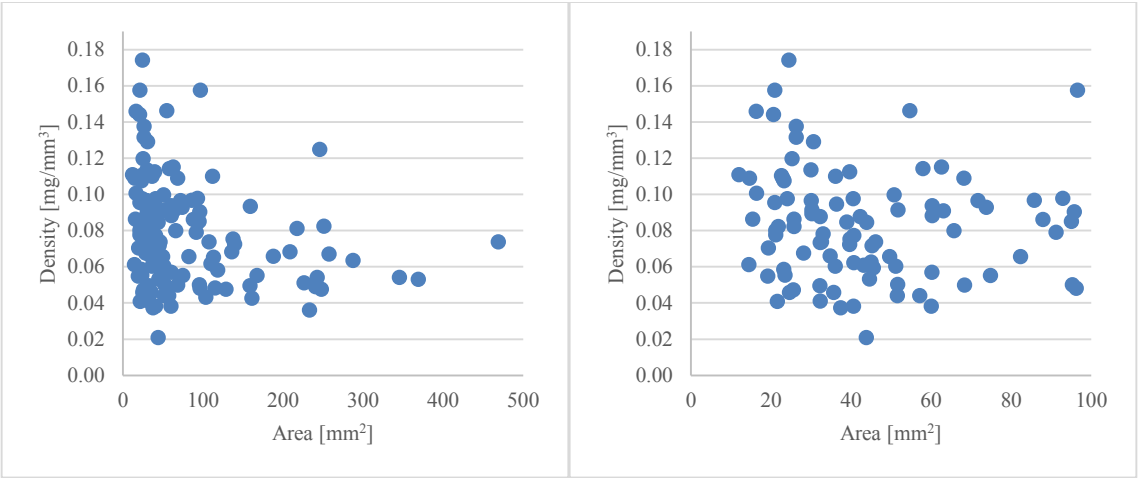


Figure 3.2. Density vs Area. Bark collected in ember plots 1 and 3. The graph on the left only shows 95% of the embers as sorted by area. The graph on the right shows scatter of data for area < 100 mm$^2$.

### 3.1.2 Study of Bark. E2.

For ember plot 2, the area was measured in a more accurate way. Using computer software we were able to determine the size of the particles with an accuracy that depended only on the pixel size. This methodology allowed our team to work with a much larger number of particles than before, mainly because the time it took for each particle to be measured was significantly reduced.

Figure 3.3 shows mass values for all particles collected in plot 2 depending on their size. Particles in red and green on the graph on the left show a much higher mass than the rest. It is possible that the three clearly separated categories of particle relate very close to the severity of burning for each piece. Since all bark pieces that were measured in this plot were photographed and identified, we can re-analyze them individually to understand this behavior. 1028 bark pieces were measured in ember plot 2. 50 of them (4.8%) are presented in the graph with red or green colors. Out of those, 44 were collected from pan 2.

A qualitative analysis of the photographs show that most of the bark pieces do look burnt (or partially burnt). Therefore their higher mass doesn't seem to be associated to their degree of burning. It seems that higher masses are associated to multiple slices of bark that were ripped of the three during or after burning and landed on the pans. The fact that almost all of them are located in the same pan (pan 2) for plot 2 could indicate that they all originated from the same three and had a similar trajectory. How this ember slices are torn from the trunk of the trees has not been completely understood, but it is likely that the presence of single slice bark or multiple

slices will depend on characteristic of the tree itself as well as on how the fire front affects each individual tree. Since there are no individual measurements of thickness for the bark collected in E2, it becomes difficult to prove this conclusion. An option would be to analyze the behavior of the mass/thickness relation of the particles by size, by using average densities for a mass range. However, this still requires repeated measurements on thick particles and these were only collected in E2.

In figure 3.3, the graph on the right shows data for all particles with an area < 150 mm$^2$ and a mass < 50 mg. This includes 664 pieces (66%). This graphs shows a range of masses for particles of the same area. Even though it is possible to see an upward trend (higher masses for bigger particles) it is likely that in this case, the difference is due to an uneven mass loss of the particle during transport. Assuming all particles share the same geometry, this would be a direct consequence of fire intensity and transport time.

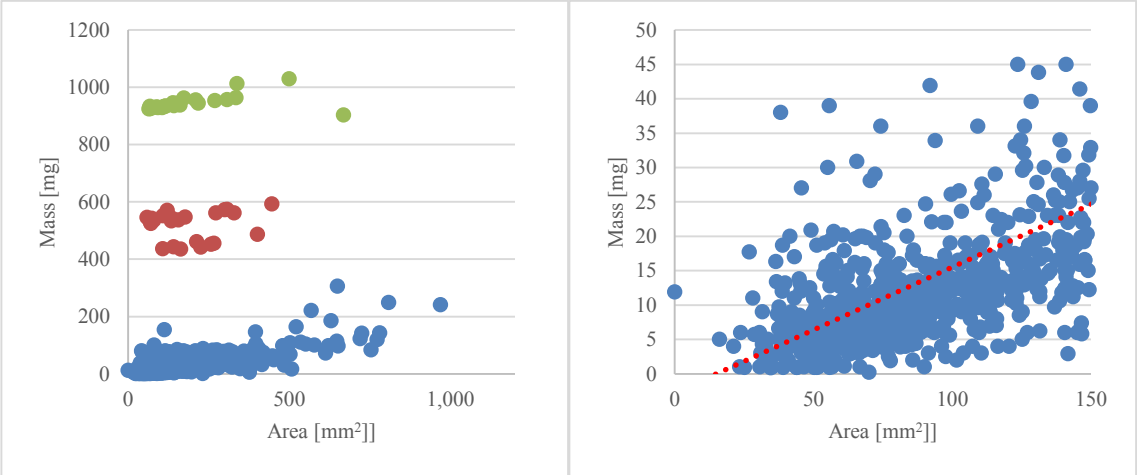


Figure 3.3. Mass vs area for all bark collected in ember plot 2. Figure in the left shows all 1028 particles. Figure in the right shows particles with an area < 150 mm$^2$ and t < 0.10 mm.

For ember plot 2, a total of 89 bark pieces, 8.65% of all barks collected in E2, were taken back to the lab and their thickness was measured. They were again divided by area categories and also analyzed independently. The independent analysis on all embers (See Figure A.7 and table A.4 in Appendix A) shows that 59.3% of all particles have a thickness between 0.5 mm and 2 mm, and also that 98.84% present a thickness of 3.5 mm or less.

Figure 3.4 shows a summary of thickness measured in all plots. Average values for thickness in plot 2 (red bars) are 20% to 70% higher than those reported for plots 1 and 3. Maximum

thickness values are 9% to 90% higher. Although this may be due to physical conditions during the fire, it is not possible to say that the samples taken from Ember 2 constitute a real statistical sample out of which extrapolation can be made. We will then use averaged, maximum and minimum values derived from data in all three plots to calculate density of each ember in plot 2.

The percentage lines in Figure 3.4 show how the particles are distributed in the different area categories for the two cases studies (E1&E3 and E2). In this sense, for E1&E3, 77% percent of all bark pieces have an area of 0-100 $mm^2$ when compared to 45% of the sample particles taken in E2. The reason to show this values is to facilitate understanding on the input of each category to the average values. It also makes sense that the particles in E2 are better distributed since they were consciously taken to represent as many sizes as possible for the lab measurements.

A possible explanation for the increase of average thickness with the surface of the particle can be the separation and break up of embers. It is possible that bigger particles are ripped from the trees by the flame front or during post-fire smoldering, and when this happens they could be constituted by single or multiple slices of bark. During transport, if the slices of bark separate into single slices, the thickness will decrease and the ember will heat up faster, increasing the mass loss. It seems that for bigger particles, it is more likely that they remain as multiple slices of bark and then their overall thickness will be higher.

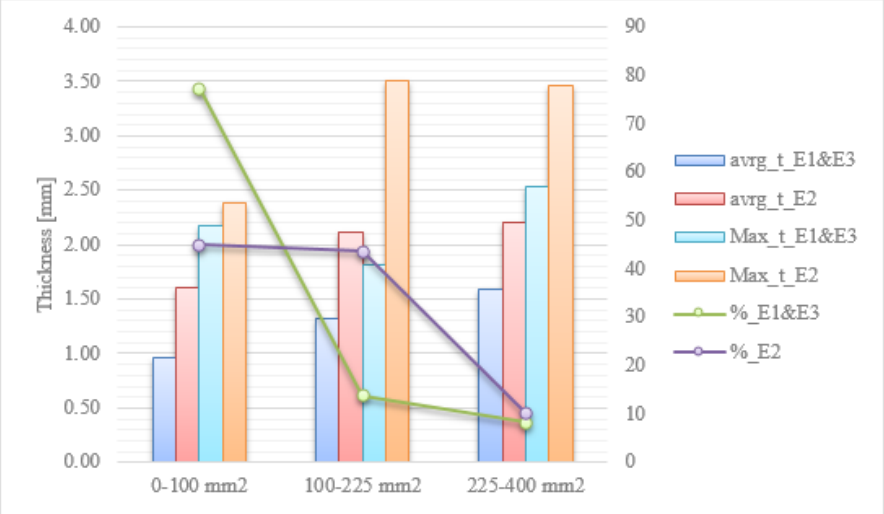


Figure 3.4. Average and maximum thickness values depending on the surface are for plots 1 and 3 (dark and light blue) and plot 2 (red and orange).

### 3.1.3 Study of Branches

The effect of the different measuring techniques is lower for the branches. For all plots, the diameter was measured manually; therefore this value is not impacted by the change in procedure. Values agree very well with [5]. 93.66% of all branches are between 2 and 6 mm in diameter and only 12.44% of them have a diameter of 2 mm or less. As concluded from the 2013 experiments, this means that most of the latter particles are consumed before reaching the collecting pans. However, most particles with a diameter lower than 6 mm are not completely consumed.

The data from the shrub consumption has not been completely analyzed for the 2014 experiments, but some differences with the 2013 conclusions can be appreciated since a big percentage of all branches collected (27.53%) fall under the $S_3$ category, which means that although they may be "less likely to ignite" [5], they will burn and turn into firebrands. This is very much affected by fire intensity and wind conditions, since vegetation remains generally similar between 2013 and 2014 (in characteristics if not in fuel load).

For plots 1 and 3, the length was measured manually and then the surface area was calculated assuming a perfect cylinder. For plot 2, the surface area was determined with the use of the software. In this situation, there is an intrinsic error in the measurement technique used in E2, and that is because the exposed, three dimensional area of a cylinder (calculated as the area of the side plus the areas of top and bottom) is actually being projected into a two dimensional surface when the software is calculating it. We then calculated the surface area as two times the area given by the software plus the top and bottom areas (which can be calculated assuming a constant diameter for the branch). There are, then, two main sources of error in the area:

a. The assumption of a perfect cylinder: the diameter was only measured once for each particle, and even though all branches do show a cylindrical shape, their real volume will change for every one of them and unless an individual analysis is made, there is no way to currently estimate an average error value. This applies to all ember plots, however, even though for ember plot 2 the same methodology is used, the photographic record does permit the verification of this assumption for each independent branch (this is not done in this report).

b. For particles in ember plot 2, the area calculated by the software constitutes a two dimensional projection of the three dimensional branch. This causes an underestimation of the side area that, although small, is present in all branches in this plot.

Table 3.2. Number of particles and percentage according to their diameter (mm). Diameter shows intervals (2 shows 0-2 mm, 3 shows 2-3, etc.)

| Diameter | # | % | Cumulative % | Color |
|---|---|---|---|---|
| 2 | 51 | 12.409 | 12.409 | |
| 3 | 110 | 26.76 | 39.17 | |
| 4 | 110 | 26.76 | 65.94 | |
| 6 | 113 | 27.49 | 93.43 | |
| 11 | 27 | 6.57 | 100.00 | |

Table 3.2 shows a summary of an analysis extended in graphs 3.5 and 3.6. When collecting the data on branches for all plots, particles of all sizes and weight were collected. The minimum mass recorded is 0.9 mg (two particles) and the maximum is 7000 mg. The data shown in Table 3.2 defines the approach taken to analyze the collection of branches. Five categories were defined according to the measured diameter: 0-2 mm, 2-3 mm, 3-4 mm, 4-6 mm and 6-10 mm. The color coding that is shown was applied for figures 3.5 and 3.6. Color blue represents $S_1$ branches, colors red and green $S_2$ branches and color purple $S_3$. Color beige represents any branch with a diameter larger than 6 mm.

In figure 3.5 left we can see the mass for all particles with an area of 500 $mm^2$ or less. This corresponds to 95% percent of them. With some minor exceptions, the particles with the smallest diameter (blue dots) show also a smaller mass. Seeing that they only represent 12% of all the branches collected, it is possible that thin particles tend to burn completely and for this reason do not land as burning embers. Also, longer branches with a thin diameter are likely to break during transport or landing resulting in a lower individual mass.

In general, higher masses are presented by green ($S_2$), purple ($S_3$) and beige branches. There doesn't seem to be much difference between purple and green particles, but it is clear that ticker particles do show a small surface area. This could be due to the fact that thicker particles weigh more and the buoyant force generated by the plume may only lift shorter branches.

The figure 3.5 on the right shows a big scatter on blue particles. Because of their size, and assuming that particles of this diameter are usually fully consumed, particles with high mass

could indicate unburnt or partially burnt particles that landed in the pans (low burning time); which would explain their presence and would reinforce the theory that usually $S_1$ branches are fully consumed.

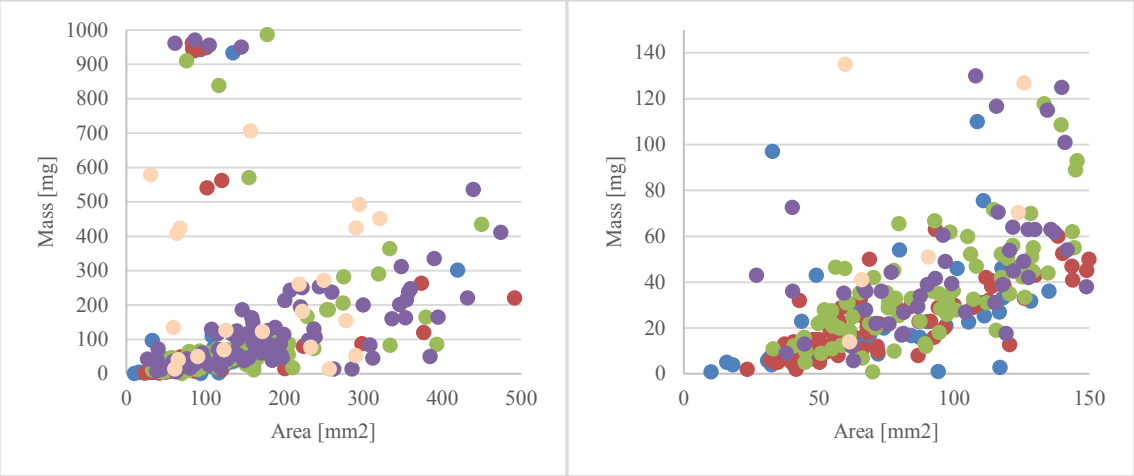


Figure 3.5. Mass vs area for all branches collected. Color coding in accordance with categories shown in Table 3.2.

Since there is still no data available on canopy consumption around ember plots, this is not being considered. However, it is possibility that if crowning happened, then the firebrand generation will be affected and perhaps that could explain the presence of thicker branches in the ember plots since a crowning fire would result in firebrand generation at 10 to 12 meters from the ground.

Figure 3.6 shows a similar comparison as Figure 3.5, but presenting density of the branches depending on their size. The graphs on the left shows two clear phenomena: First, blue particles with an overall higher density than the average of the other colors which, again, supports the argument that small thinner particles present in the pans could land partially burnt (complete graph can be seen in Appendix A. Figure A.8). Also, Beige particles (thicker) seem to have lower densities, which could indicate a higher mass loss. This could be due to the fact that, as was already seen, thicker particles that are lifted seem to be shorter than the rest. It is possible that this particles burned during the approach of the fire front and then were lifted by the plume only when their mass loss was sufficient to generate a mass low enough to be lifted by the plume. On this sense, their lower densities would be a result of burning caused by the fire front and burning during transport after lifted.

For the graph on the right, particles with an area < 150 $mm^2$ and a density < 0.1 $mg/mm^3$ are shown. This corresponds to approximately 70% of all particles. It is interesting to see that the thinner particles (blue dots) show, in average, higher densities than red, green, purple and beige particles. In fact, purple and beige particles (thicker) show lower density values than red or green particles, which follows the explication above.

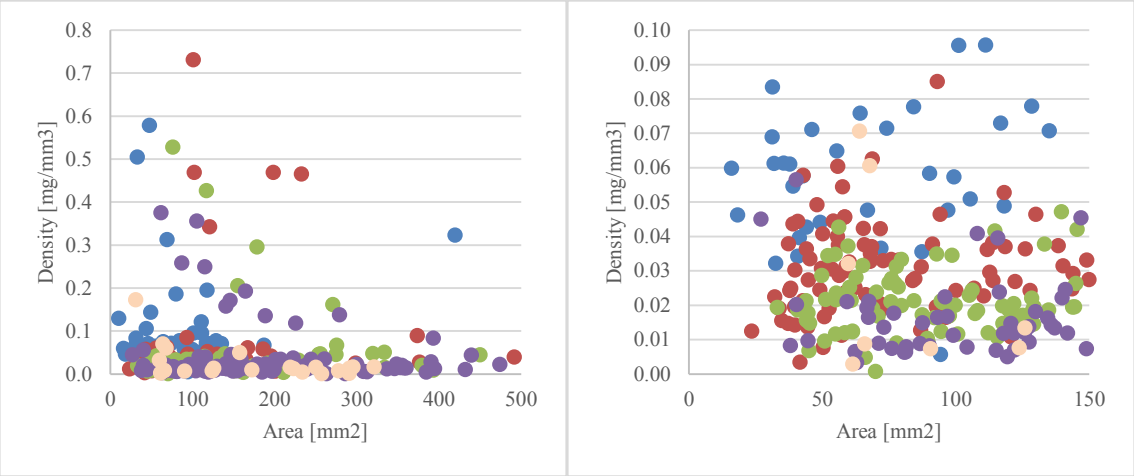


Figure 3.6. Density vs area for all branches collected. Color coding in accordance with categories shown in Table XX.

### 3.1.4 Impact of fire behavior

Calculations on wind behavior and fire intensity are only used in this report to support the analysis, but they were not done under the framework of this thesis and the information is reproduced with permission of the authors.

- **Wind velocity**

Figure 3.7 shows the wind magnitude and direction close to understory tower 3, which is the closest measurement tower from ember plot 1. Wind velocity measurements were taken by bi-directional probes at a height of 1.5 meters. The gray dots show instantaneous measurements, taken at 50 Hz, and the black line shows a Loess type smoothing algorithm that uses a 20 second span. Figures A.10 and A.11 in Appendix A show the same figures for the towers positioned closer to ember plots 2 and 3.

For the velocity measurements on a bi-directional probe, a reference temperature is needed. In the case of the measurements for ember plot 2, the reference thermocouple did not function properly during the test. For this reason, two figures (A.9 and A.10 in Appendix A) were created. The first one uses the faulty thermocouple and for the second one, a thermocouple from

a close tower was used, shifting the readings back in time to accommodate the distance between the two towers. The two graphs seem quite similar, and the main influence of the change in the thermocouple reading is in the peak velocity during impact of the flame front. The direction shows were the wind is heading (as oppose to some meteorological conventions that show were the wind is coming from). Degrees are compass degrees, which mean that 0/360º indicates the North and that it increases clockwise (90º is East, 180º South and 270º West).

For ember plot 1, maximum winds of 12-14 m/s were instantaneously recorded but, peaks on the smoothing graph show values between 8 – 10 m/s. It is possible to see an initial period of ambient winds, with low magnitudes and fluctuating directions. Once the fire front reaches the tower, winds align to the North (entrainment) and then, after the peak, the winds align towards the departing fire with an average velocity of 3.6  m/s (STD of 1.7 m/s), which is comparable to 2013 [5].

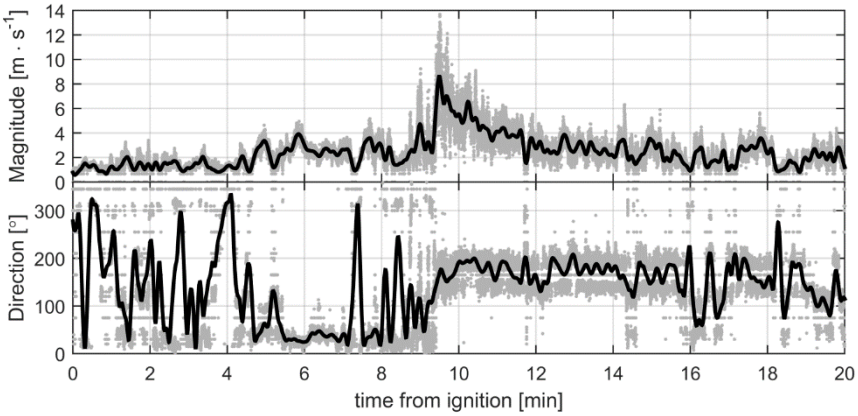


Figure 3.7. Wind magnitude and direction. Understory tower 3, close to ember plot 1. Reproduced with permission.

On the case of ember plot 2, using Figure A.10 (shifted temperature readings from working thermocouple), a similar behavior is evidenced. Maximum (smoothed) magnitudes range between 8 – 10 m/s and the wind generated after the fire front has an average magnitude of 3.3 m/s (STD of 1.8 m/s). This is somewhat lower than ember plot 1, but in any case values are very similar. It does not explain the difference in the number of embers collected (even considering those that were not independently measured in plot 1).

For ember plot 3 (Figure A.11) the information shown is different. The wind displayed is mostly lead up since the fire does not reach the tower until after 20 minutes have passed. The readings in this location come from the overstory tower located outside of the fire perimeter and a sonic

anemometer is used to measure wind speed at 2 meters height. There is a period of strong winds towards the west/south west after 10 minutes, which seems to be a consequence of the intense fire occurring at plot 2 at that time. As mentioned, both the tower and the ember plot are located outside of the fire perimeter and this relates to ember collection results since particles collected were the lowest in mass and quantity out of the three plots.

- **Fire intensity**

Table A.6 shows fire intensity at different locations. The distance refers to the fire contours shown in Figure 3.8. Higher fire intensities will undoubtedly results in the generation of more embers. Intensities of the fire are comparable, although somewhat higher, than what was calculated in 2013 [12]. Values mentioned in this table only represent surface fire intensity and any consumption of canopy fuels is not taken into account.

From the figure, we can see that the fire impacts the ember plots in succession (E1 then E2 and finally E3). Fire intensity calculated for E1 is around 40% higher than for E2. It is strange to see that both wind speed and fire intensity were higher for E1 but the number of embers collected is much higher in E2. It is possible that the reason for this is the way the fire spread inside of the plot with regards to the location of each ember plot. An analysis of the contours shown in figure 3.8 reveals that there is a backward “peak” in the way the fire advances trough the plot. This is because there is a service road in the middle used for the fire fighters that acts as a fuel break. E1 is located much closer to this road than E2.

Another possible factor is the way post-fire smouldering affects the creating of embers. As it was mentioned, wind direction aligns with fire spread after the flame front has gone through a given location. Since E2 is located farther into the plot than E1 (which was positioned closer to the ignition line), there is clearly much more fuel (trees) affected by post-fire smouldering that could create embers. Also, other factors may be affecting the production of embers, such as the density of the vegetation around each plot or whether or not crowning was observed.

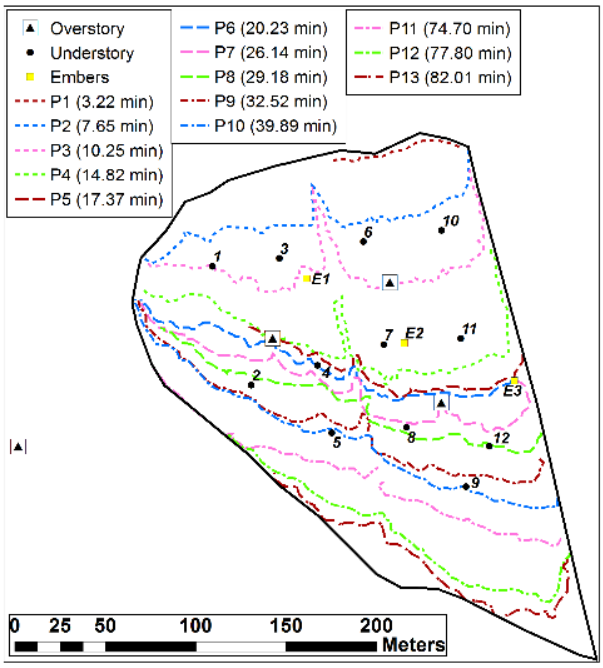


Figure 3.8. Fire contours that show fire progression for different times. Reproduced with permission.

## 3.2 Small scale laboratory experiments. Analysis of ignition of wood by conduction.

Tables 3.3 and 3.4 show a summary of all the experiments performed. In table 3.1 all the category 1 experiments (heater + wood) are summarized. The first two set of experiments (1-3 and 4-6) were done to understand the capabilities and limitations of the use of the electrical heater. The analysis of the results presented for these experiments is based on the understanding of the phenomenon and the limitations associated to measuring surface temperature as well as the effects of the thermal attack and the wood decomposition (including cracking) on the heat transfer process.

Table 3.3. Experiments conducted with the heater on wood. Category 1.

| Experiment # | Voltage | Direction of the heater | Insulation | Thermocouple | Heater on [min] |
|---|---|---|---|---|---|
| 1 | 60 | Parallel | No | Yes (1) | 76 |
| 2 | 90 | Parallel | No | Yes (1) | 110 |
| 3 | 120 | Parallel | No | Yes (1) | 115 |
| 4 | 60 | Parallel | No | No | 86 |
| 5 | 90 | Parallel | No | No | 95 |
| 6 | 120 | Parallel | No | No | 78 |
| 7 | 60 | Parallel | Yes | No | 30 |
| 8 | 90 | Parallel | Yes | No | 30 |
| 9 | 120 | Parallel | Yes | No | 30 |
| 10 | 60 | Parallel | Yes | Yes (2) | 30 |
| 11 | 90 | Parallel | Yes | Yes (2) | 30 |
| 12 | 120 | Parallel | Yes | Yes (2) | 30 |
| 13 | 60 | Perpendicular | No | No | 30 |
| 14 | 90 | Perpendicular | No | No | 30 |
| 15 | 120 | Perpendicular | No | No | 30 |

Table 3.4. Experiments conducted with the heater on vermiculite. Category 2.

| Experiment # | Voltage | Direction of the heater | Insulation | Thermocouple | Heater on [min] |
|---|---|---|---|---|---|
| 16 | 60 | Parallel | No | Yes (3) | 30 |
| 17 | 70 | Parallel | No | Yes (3) | 30 |
| 18 | 80 | Parallel | No | Yes (3) | 30 |
| 19 | 90 | Parallel | No | Yes (3) | 30 |
| 20 | 100 | Parallel | No | Yes (3) | 30 |
| 21 | 110 | Parallel | No | Yes (3) | 30 |
| 22 | 120 | Parallel | No | Yes (3) | 30 |

As explained before, figures 2.4 and 2.5 show the location and distance to the surface of every thermocouple installed. Thermocouples F (3mm), G (6 mm) and H (9 mm), located at a distance of 5 mm from the edge will represent Section 1. Thermocouples I (3 mm), J (6 mm) and K (9 mm), located at a distance of 30 mm from the edge represent Section 2. Temperature profiles over these TCs show the thermal penetration trough the wood (from top to bottom), in direction x.

Appendix B shows the temperature profiles derived from all the experiments performed. In Appendix B.1 to B.15, four graphs are shown for every experiment. The top graphs display the temperature profiles trough the wood in sections 1 and 2. The bottom ones show temperature profiles, at a depth of 6 mm from the surface, in the y (perpendicular to the grain) and z (parallel to the grain) directions. Surface temperatures were measured in two out of the 4 sets of experiments. When the surface temperature is available, the heat flux (x direction) will be calculated using Fourier's law, assuming a one dimensional situation and homogeneity of the wood in that direction. Also, a constant conductivity of the wood is considered (the reasoning for this assumption is expanded below).

### 3.2.1 Experiments 1-6.

Figure 3.9 shows the time it took to reach 100 ºC in the most superficial thermocouple, for experiments 1-6. Bars in red show time for the "F" location (section 1). Bars in blue for the "I" location (section 2). Solid bars show results for experiments 1-3 and patterned for 4-6. In experiments 1-3, an exposed thermocouple was placed between the surface of the heater and the wood. This affects the results in two ways: first, the presence of the thermocouple alters the conduction between the heater and the wood since the contact surface becomes less effective, and second, the small separation between the two surfaces created by the thermocouples facilitates the inflow of air. It can be seen from figure 3.9 that the heat transfer seems to have a better repeatability in section 2.

Indeed, a qualitative analysis of the samples after the test showed that the heating of the wood was much more irregular in section 1, and this is because it is much harder to ensure a perfect contact of the heater in the edge. Also, closer to the edge the heat losses increase and due to the presence of the thermocouple, the contact surface was reduced. However, experiments 1 and 3 show results that are counter intuitive (red columns for 60 V). When there is no surface thermocouple, the contact between the heater and the wood should improve and the heating should be more effective, reaching 100 °C faster. The reason it took longer in experiment 3 is because it was found that the heating area of the electrical heater is smaller than initially assumed. Even though the full length of the heater is 13 cm (width of 4.5 cm), the actual heating area is only 5 cm (width of 4.5 cm), therefore the heated area was not properly aligned with the center area of the sample.

The reason behind discussing this graph is to analyze the applicability of the one dimensional assumption when considering heat transfer. We assume that in the area where the thermocouples are located, heat propagates trough the wood (x direction) in a uniform way, so the isothermal lines should be parallel to the surface. This is clearly not the case, and even less for lower heat fluxes.

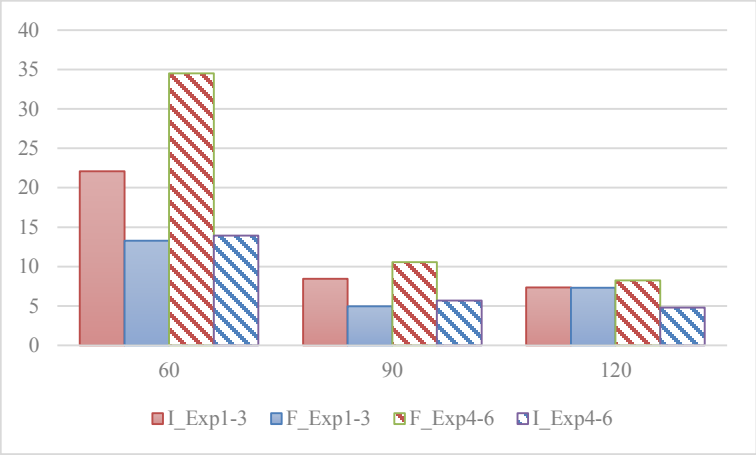


Figure 3.9. Time (min) to reach 100 ºC for 3 mm deep thermocouples (Sections 1 and 2). Experiments 1-6.

Figure 3.10 shows temperature profiles, trough the wood, for experiments 1-6 in section 2 (thermocouples IJK). The dotted line in the first three graphs represents the surface temperature measured by one single, exposed thermocouple. Even though all the lines are shown for the complete experiment, it is very important to highlight that, contrary to other experiments in the literature (which study radiation), the study of conduction is extremely sensible to the degradation process of the wood. Following convention on the field [8], we will consider that the charring temperature of the wood is 300 °C. It is common to assume that the solid is inert until this temperature is reached. This is clearly not the case.

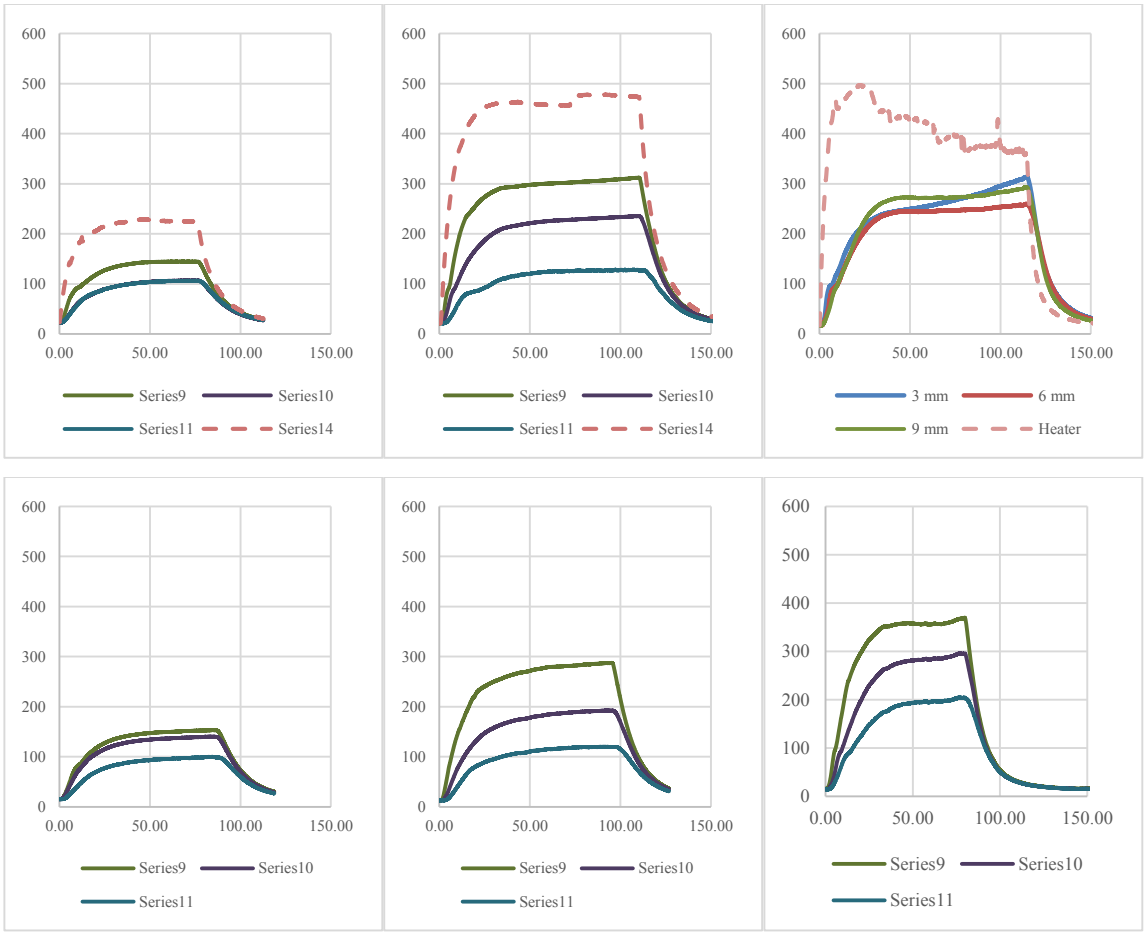


Figure 3.10. Temperature profile. X direction. Section 2. Top: Experiments 1, 2 & 3. Bottom: Experiments 4, 5 & 6.

The top left and bottom left graphs in figure 3.10 show the temperature profile for a heater setting of 60 V. The behavior is very similar. The surface temperature follows a rapid increase and then a plateau around 230 °C. 3 mm deep thermocouples are very similar for both experiments. However, the 6 mm deep thermocouple (J) shows much lower temperatures for experiment 1 (blue line, K thermocouple) than in experiment 4. It is probable that the thermocouple moved during the final preparations. Initial tests (1-6) did not fix the thermocouple at the holes so it could have been pulled out of its position, showing readings for a greater distance to the surface.

Top center and bottom center show temperature profiles for experiments 2 and 5. It is possible to see the effect of cracking and shrinkage in the wood. The heater increases its temperature as long as it hasn't reached an equilibrium state. However, we can see that around 50 minutes there is a gradual decay in the "surface" temperature which reaches a local minimum at 71 minutes, and

then it increases again. At 50 minutes the temperature at 3 mm has already reached 300 °C, which means that, in this point, there exist 3 mm of char already. An analysis on the samples shows that at a 90 V setting, there is localized charring, but it reaches a limited depth. Most likely, the decrease in the temperature is due to air coming in and cooling the tip of the thermocouple. However, as the temperature in the wood increases, the air flow eventually facilitates glowing combustion (observed during experiments) and this causes an increase of the temperature around the thermocouple. This would also explain the higher temperatures at 3 mm for experiment 2 than for experiment 5. In experiments where an exposed, surface thermocouple was used, glowing combustion appeared first. Clearly, this initial design to measure surface temperature is flawed, since it strongly impacts the heat transfer.

Finally, for the two cases with a setting of 120 V the results are less reliable. The surface temperature reaches 500 °C very quickly. No flaming ignition is observed, but the thermal penetration in the wood causes a high charring rate with an immediate impact in the surface. Charring causes the wood to shrink and the thermocouple separates from the heater, which explains the temperature drop. At that moment, the heat flux into the wood decreases dramatically, and this is because the contact is much less effective, so the losses at the surface increase considerably. This reasoning is supported by experiment 6. Since there is no thermocouple, there is no localized point where glowing combustion can start easily (as in the case of experiment 3). The separation between the heater and the wood happens at a later stage and temperatures reach higher values.

Two other factors need to be mentioned on the results for experiments 3 (top, right). First, the fact that the lines between the temperatures at different depths are so close from each other, which could be due to the fact that the thermocouples (specially 3 mm and 6 mm) moved during installation and they actually measure temperatures farther from the surface. It is also possible that, since the holes used for the thermocouples in this experiment are of a bigger diameter (2.5 mm), then at high heat fluxes the charring rate is accelerated by the intake of oxygen through the holes when the temperatures are high enough. In other words, temperatures inside of the thermocouple hole could be higher than the sample temperature. This is observed as localized blackening (does not reach charring) of the sample's surface in the opposite face to the heater around the thermocouple holes. Finally, the fact that the temperature lines cross would seem strange since thermocouples closer to the surface should have a higher temperature. This is merely a consequence of the advancement of the charring rate where, at high heat fluxes, the

depth of penetration is such that the lower thermocouple can be affected by the glowing combustion while the higher thermocouple is exposed to cooling due to cracks in the wood.

Experiments 1-6 served to determine that the heater could provide enough energy to produce charring in the wood and reach temperatures of interest, as well as to prove that the method to measure surface temperatures in experiments 1-3 affects the results in an unacceptable manner. Only section 2 was studied since it provided more stable results. The study of the edge will be critical for the understanding of the situation (since ignition is always seen to start on the edge in ember trials) but it was not considered in this first approximation because the one dimensional assumption was proven not to be applicable. Also, as expected, it was shown that it is really hard to quantify the effect of pure conduction in the wood since, when the temperatures increase, the wood starts to degrade which in turns affects the surface geometry and reduces the surface of contact.

### 3.2.2 Experiments 7-12.

In experiments 7-12 the wood sample was completely insulated. A heating time of 30 minutes was chosen for all experiments. The goal is to study the thermal penetration of the wood with a better controlled situation.

Figure 3.11 shows the difference in time to reach 100 °C for thermocouples F&J (3 mm), for experiments 4-6 and 7-9. The larger the difference, the less valid the one dimensional heat transfer assumption can be considered. The fact that the difference in the time to reach 100 °C is so drastically reduced is a great indication that by insulating the wood the isothermal lines align much better with the surface of the sample. For this reason, the comparisons made with other experiments are done by using the values from experiments 9-12, where insulated samples of wood are exposed to the heater and surface temperatures were measured.

The maximum temperatures reached for exp_7-9 are 32% and 44% higher for 60V and 90V, respectively. For 120V, the maximum temperature closer to the edge is lower for the insulated case. This is because in the non-insulated case (exp_6), the experiment was continued until glowing combustion was observed, and the charring penetration was higher closer to the edge. Glowing combustion was more intense were there was an inflow of air (closer to the edge) and this explains the higher readings in the F thermocouple for experiment 6 (non-insulated) than for experiment 9 (insulated). The average heating time for exp_7-9 is 60% lower than in the

previous set, so maximum temperatures can't be directly compared but the qualitative analysis shown above explains the impact of insulation in the thermal penetration.

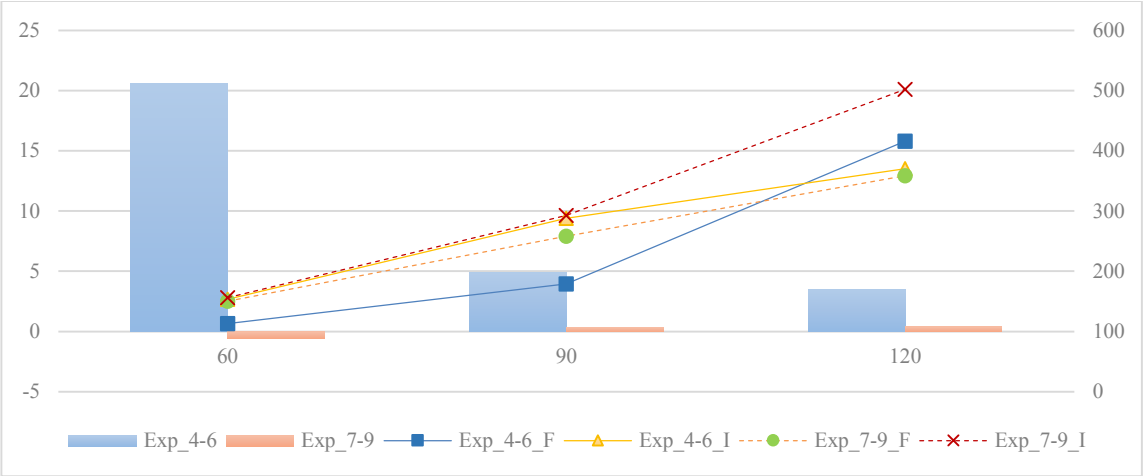


Figure 3.11. Columns: Difference in time to reach 100 °C for surface thermocouples (F-J). Lines: Maximum temperature reached.

The solid and dashed lines in figure 3.11 show the maximum temperatures at both locations for the two sets of experiments. The dashed lines show values for the insulated samples, and it can be seen that the difference between the maximum temperatures is smaller for this case. With the exception of 120 V (for the reason explained above).

Figure 3.12 shows temperature profiles trough the wood (x direction) in section 1 and section 2, for experiments 8 and 11 (90V). For experiments 9-12, a different, less invasive method was used for measuring the surface temperature. Sheathed thermocouples with a diameter of 0.2 mm were positioned into shallow channels (< 1 mm deep) to be able to fix the thermocouple at a repeatable location. Contrary to experiments 1-3, where the thermocouple was inserted from the side (90°); in these experiments the channel to insert the thermocouple was made in alignment with the heater. This was done with the intention to decrease the influence of the thermocouple on the charring rate of the wood. Two surface thermocouples were installed, at 10 and 20 mm from the edge, at lengths of 120 and 140 mm (the samples are 260 mm long). The dashed lines in figure 3.12 show these readings.

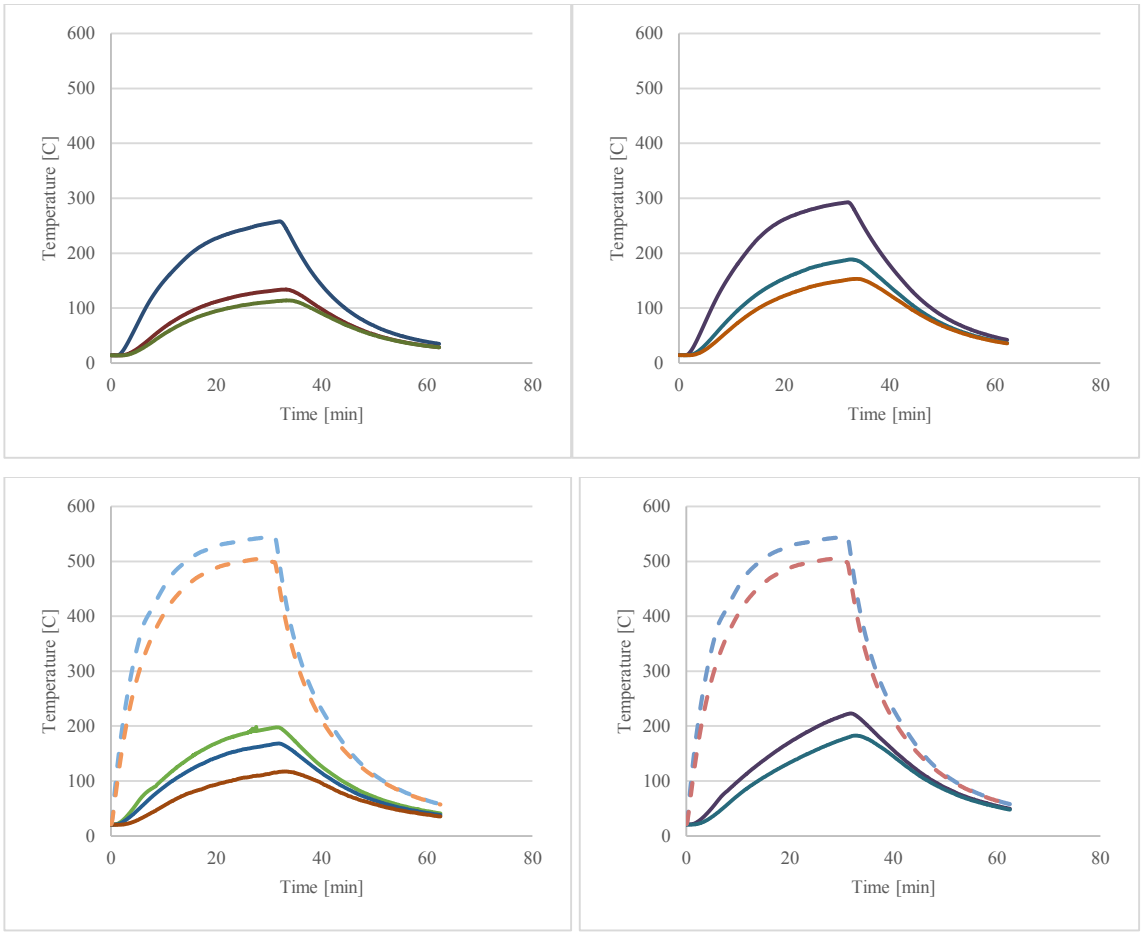


Figure 3.12. Temperature profiles trough the wood. Top: Experiment 8 (90V). Bottom: Experiment 11 (90V). Dashed lines represent surface thermocouples.

All curves show temperature profiles for a heater setting of 90V. Comparing top and bottom graphs, experiment 8 registered temperatures 22-27% higher than in experiment 11. Surface temperature readings are somewhat higher than what was measured in experiment 5, which is logical since the sample is insulated. The overall behavior in both experiments is very similar and the impact of the measurements for surface temperature has been reduced by using thinner thermocouples and inserting them in alignment with the heater (as opposed as trough the edge).

To summarize, it can be said that figure 3.11 shows the impact of the insulation of the wood samples and the way it improves the heat transfer situation with respect to the one dimensional assumption that was made to simplify the study of the problem. From figure 3.12 it can be seen that the second method to measure surface temperatures has had a lesser impact on the heat transfer and thus, it will be used for comparisons with other experiments.

### 3.2.3 Experiments 13-15.

Experiments 13-15 allow for a qualitative analysis on the influence of the grain direction on the heat transfer process. Contrary to other experiments, in this set the heater was placed perpendicular to the direction of the grain. Figure 2.5 shows the way the thermocouples were used for this configuration. The comparison is made between experiments 4-6 (non-insulated, heater parallel to the grain) and 13-15 (non-insulated, heater perpendicular to the grain). Only the first 80 minutes are shown (exp_4-6 did not have a heating limit of 30 minutes) but it is assumed than once a temperature of 300 °C is reached, the data is not valid anymore.

Figure 3.13 shows the temperature profile obtained in this direction for both set of experiments. All readings are for thermocouples located at 6 mm from the surface. No surface temperature measurements were made but it wouldn't have been possible, with the tools used in this report, to calculate a heat flux parallel to the surface since, by its own nature, this is a 2-D dimensional problem. So, for the purpose of this thesis, only a qualitative analysis is performed on the temperature evolution.

There is also another factor that limits the applicability of this analysis, the boundary conditions. The wood sample has a rectangular shape, 260 mm by 150 mm. The heater has a length of 130 mm. When the heater is aligned parallel to the grain (exp_4-6, top graphs), then the edges of the heater are located 65 mm away from the edge of the sample. However, for experiments 13-15, the situation is different. The heater is then assumed to share three edges with the sample and the losses increase.

The green line in all the graphs shows temperature for thermocouple C (15 mm from the edge), purple line for thermocouple J (30 mm from the edge) and orange line for thermocouple L (50 mm from the edge).

Since there is a different heating time for the two sets of experiments, we will only consider the first 30 minutes for the analysis. Experiments 4 and 13 (top left and bottom left) show the temperature evolution at 60V. The heating rate seems to be similar and the maximum temperatures are just shy of 150 °C. However, some clear differences can be highlighted. First, in experiment 4 thermocouple J shows the highest temperature, whereas in experiment 13 is thermocouple C. It was explained before that the one dimensional assumption did not apply to the first two set of experiments since temperatures were much higher in section 2 (30 mm from

the edge) than in section 1 (5 mm from the edge). From the analysis on the temperature profiles we can see that samples were not completely removed of their moisture content, and that is why local maximums are reached in the graph, then temperature remains constant for a short amount of time and then it continues to increase. The production of water vapor absorbs most of the energy for that period of time and there is no increase in the temperature until the moisture content has reached 0%.

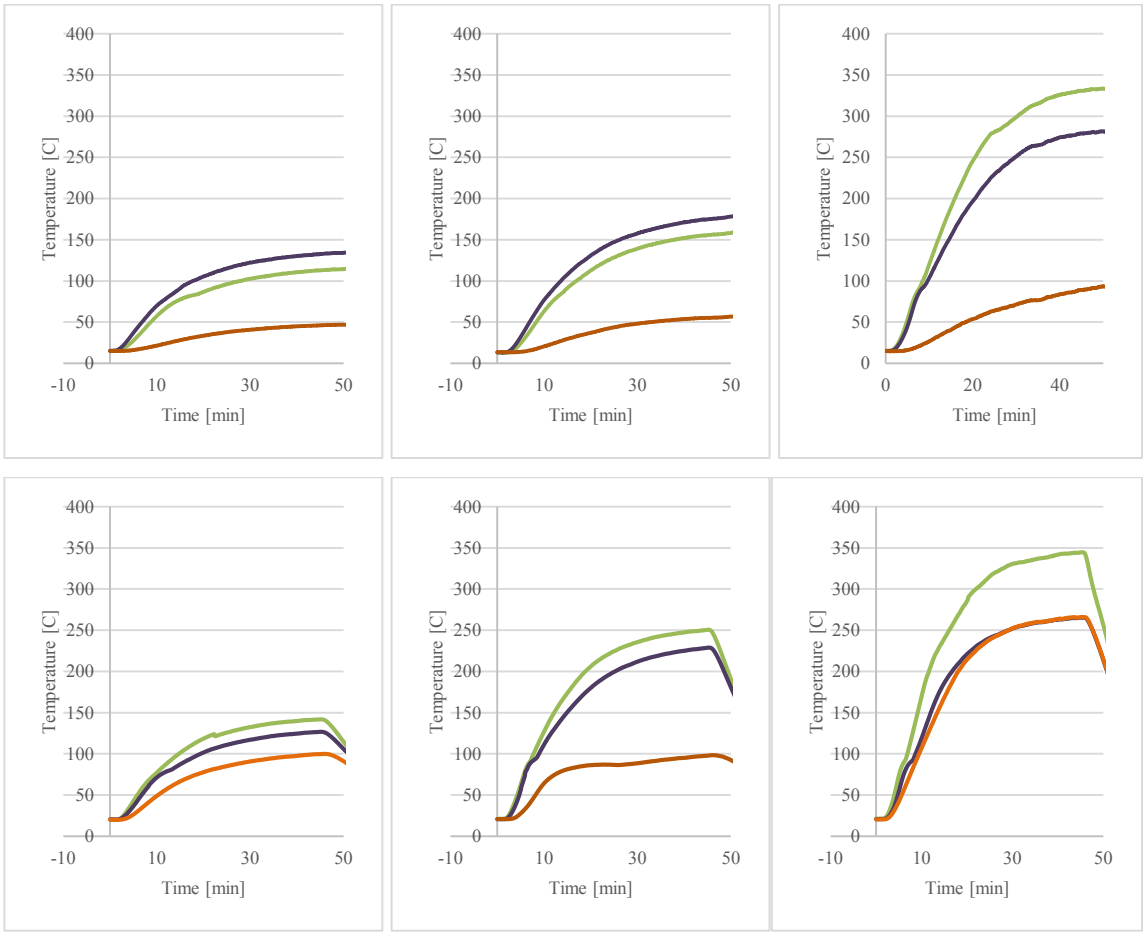


Figure 3.13. Temperature profiles for a direction of the heat flux perpendicular to the length of the heater. Top: perpendicular to the grain for experiments 4-6. Bottom: parallel to the grain for experiments 13-15.

Since both thermocouples C and J are assumed to be under the heating area of the electrical heater, it can be argued that the temperature line that better displays the effect of the grain direction is that which corresponds to thermocouple L (6 mm deep, 50 mm from the edge). In experiments 13-15 (bottom graphs), Temp_L is between 100 to 150% higher than for the equivalent experiments in 4-6. This is in accordance with what is shown by [8], where the thermal conductivity of wood is greater along the grain. In experiment 15, the lines for

thermocouples L and J show very similar temperature profiles. As has been mentioned before, in all the tests performed at 120 V it seems that the thermal attack is so intense that charring occurs in a very short time. When this happens, exothermal reactions in the wood affect the temperature profile and then it is not possible to separate the influence of only grain direction.

### 3.2.4 Experiments 16-22.

For experiments 16-22, instead of wood samples, a non-flammable, isotropic, inert material was used to study the thermal penetration caused by the heater. 7 different settings were studied: 60V, 70V, 80V, 90V, 100V, 110V and 120V. The conductivity of the material is assumed to be constant and equal to 0.1 W/m*K (as provided by the supplier). The material is commonly known as vermiculite. Figure 3.14 shows the heat flux trough the wood, from the surface to the 6 mm thermocouple (G and J). The thermocouple distribution was the same as the one used for the wood, as shown in Figure 2.4. The heater was kept on for 30 minutes and that is the time shown by all the lines.

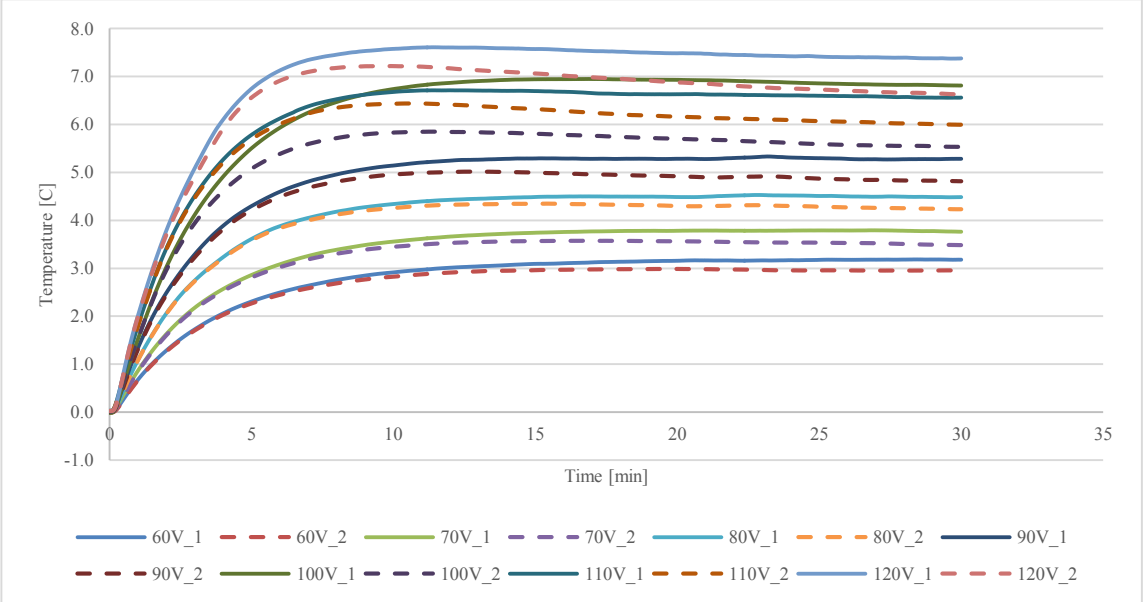


Figure 3.14. Heat flux over time for vermiculite. Solid lines show thermocouple G and dashed lines thermocouple J.

Contrary to what happens with the wood, since there is no degradation of the material the process reaches a (seemingly) steady state. The dashed lines show the temperature in thermocouple J (30 mm from the edge) and the solid line show it for thermocouple G (5 mm from the edge). The higher heat flux for a supply of 120V is close to 7.5 kW/m$^2$.

For a voltage supply of < 100V (calculated Q" at steady state of 3-5.5 kW/m$^2$), the behavior is very similar for both sections. However, as the heat flux increases the difference starts to increase also. At 30 minutes, there is a difference of ~ 10% for a supply of 120V. The higher heat fluxes in section 1 (close to the edge) are explained by the fact that for higher temperatures, the losses in the edge will increase. Since the surface temperature is assumed to be the same for all the contact surface, then lower sample temperatures (6 mm from the surface) would result in higher heat fluxes. The graph above was determined using Fourier's equation for a one dimensional problem, assuming a homogeneous material and a constant conductivity:

$$q" = k \frac{Tsurface - Tthermocouple}{0.006}$$

This results seem to indicate that the degradation of the wood caused by charring holds a much bigger relevance when analyzing the one dimensional approach in the wood than the boundary conditions at the edge. In other words, it was mentioned that observations during the experiments led to the conclusion that the contact between the heater and the wood, at the edge, is not ideal. This could lead to lower temperatures close to the edge but also, the separation may serve to create a flow of air coming into the sample. The fact that the difference between the heat fluxes is small (as shown in figure 3.14) means that this effect does not have a big influence on the heat transfer process.

### 3.2.5 Heat flux calculations and comparison with other experiments

To analyze the process of ignition of wooden structures by embers, several different factors have to be considered. The combustion process and heat transfer from the embers to the wood depend on external variables (wind, temperature, humidity), material characteristics and on the embers themselves. These studies have used an electrical heater to simulate the thermal penetration caused by the landing of hot embers. The situation reproduced can be compared to small tests performed with simulated embers on vermiculite and wood. We will use the heat flux evolution to understand the applicability of the comparisons.

Five different zones can be defined when the wood is exposed to a heat flux high enough to generate charring [8]. The study of transient heating of the wood means that the charring rate has to be determined to be able to understand the impact on the conduction inside of the material. When the heater is turned on, its thermal inertia and the thermal inertia of the sample determine the rate of temperature increase (for a given voltage) as well as the maximum temperature.

Figure 3.15 shows the temperature profile at section 1 in Experiment 2. The dashed line shows the surface temperature as measured with the initial methodology and the solid lines the thermocouple readings at 3, 6 and 9 mm. The surface temperature of the heater will not equal that of the wood, which would be lower for a given moment. The five zones that are mentioned before [8], look to describe the behavior of wood when charring is taking place. For temperatures higher than 280-300 °C, the physical structure starts to break down, cracks appear and the pyrolysis rate increases. The char also slows down the heating rate of the sample since the conductivity of the char is much less than that of virgin wood. In this report, we do not consider the evolution of the charring rate or the transition to flaming (which was not observed in the experiments performed).

We consider the heating of the wood samples until temperatures have reached 300 °C. Below this temperature, three regions can be considered: virgin wood, 100-200 °C and 200-300 °C. Above 100 °C the chemically unbound water starts to evaporate form the surface. That is not seen in figure 3.15 since, for this experiment, the samples were dried in the oven until their moisture content was close to 0%. This process absorbs energy and usually is seen as a local plateau in the graph. When the temperature reaches 160-180 °C the cellulose and hemicellulose start to decompose; this is an endothermic process and it accounts for the change of slope in the graph (lower rate of temperature increase since part of the energy is being used).

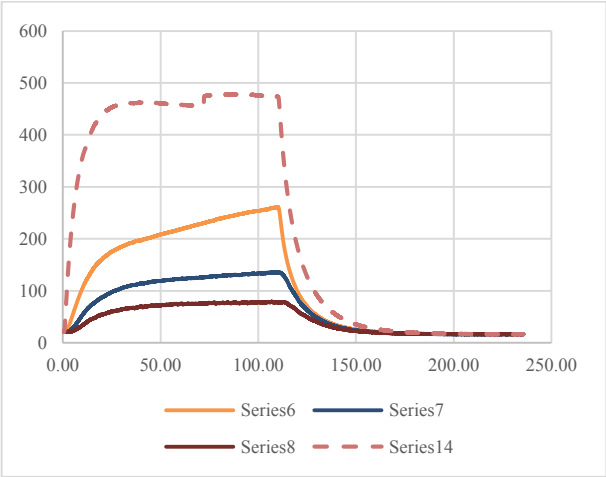


Figure 3.15. Temperature profile in section 1. Experiment 2 (90V). Dashed line shows surface temperatures.

One of the main problems that derive from these experiments is the determination of the time at which the results should not be considered anymore (the 300 °C threshold). As explained

before, the temperature at the surface of the heater will not be the temperature of the wood surface (transient conduction), so assuming that the analysis should stop when the dashed line reaches 300 could be an overly conservative assumption. It is also not correct to consider only the most superficial thermocouple since at that point, there would already exist 3 mm of charring in the sample.

Figure 3.16 shows the heat flux calculated for experiments 10 and 11 (60V and 90V, insulated samples). The dashed lines show the surface temperature as well as the temperatures of thermocouples F and I. The solid lines show the heat flux from the surface to these thermocouples. A constant conductivity of 0.13 W/m*K was used. This value resulted from a hot disk test for the determination of conductivity at 75 °C for samples of the wood (20 mm thick and 50 mm in diameter). [16] found a 15% increase in the conductivity of wood when the temperature is raised from 20 °C to 100 °C. This is not considered in the analysis. The green line in Figure 3.15 shows the time at which a temperature of 300 °C is reached by the heater. This simplified heat flux is used to compare the thermal penetration on the sample, especially at the beginning of the experiment (t < 8 min) when the temperature in the sample is below 100 °C. The conductivity of wood increases with temperature until charring is observed, at which point the wood decomposes and the conductivity decreases. Assuming a constant conductivity is not an accurate assumption if the goal is to study the parameters of ignition of wood, however, it allows us to calculate initial approximations of heat flux values that can later be used to qualitatively compare with the other set of experiments.

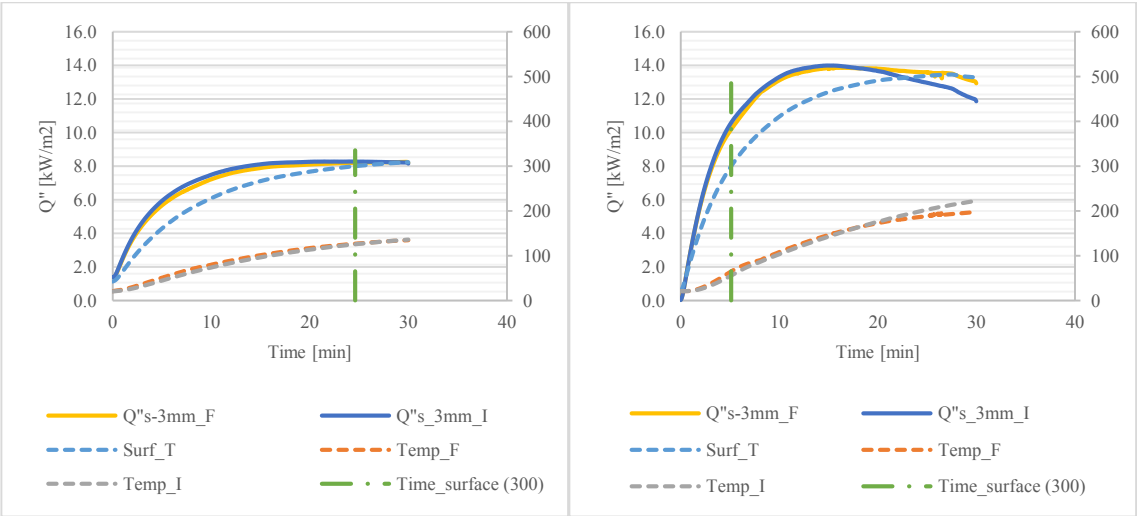


Figure 3.16. Heat flux (solid line) and temperature profiles (dashed lines – secondary axis). Left: Experiment 10 (60V). Right: Experiment 11 (90V).

Figure 3.17 shows the temperature profile for experiments conducted by placing hot embers (pieces of bark) on top of vermiculite boards. The graph on the left corresponds to experiment 26, where 60 grs of embers were used (prior to being burned). The graph on the right corresponds to experiment 28, 40 grs of embers were used. The location for the thermocouples remained the same (Figure 2.4). These experiments are shown because they represent the cases where flaming ignition was observed (exp_25) and not observed (exp_24) in experiments with redwood. The graphs on figures 3.18 show the corresponding heat fluxes calculated by assuming a constant conductivity between the surface and the 3 mm thermocouple in section 1 (5 mm from the edge).

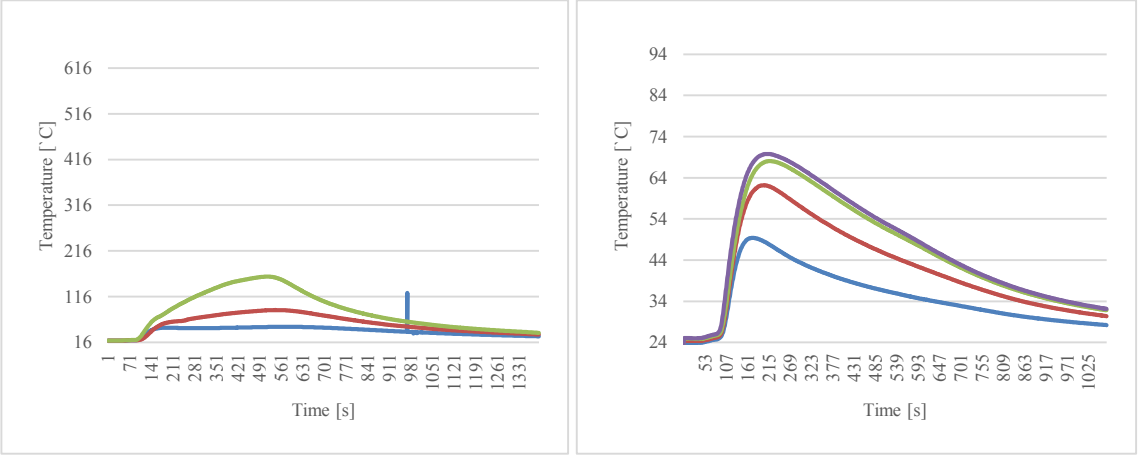


Figure 3.17. Temperature profiles. Embers on vermiculite. Experiments by Kamila Kempna. Left: Experiment 26 (60 gr). Right: Experiment 28 (40 gr). Reproduced with permission.

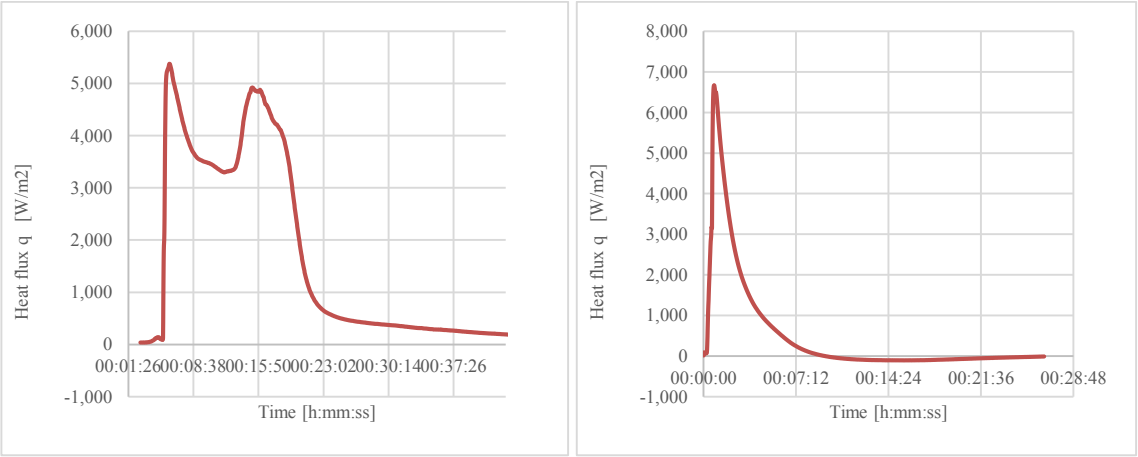


Figure 3.18. Heat flux from embers to Vermiculite. Experiments by Kamila Kempna. Left: Experiment 26 (60 gr). Right: Experiment 28 (40 gr). Reproduced with permission.

The main difference in the temperature profiles is that the temperatures in the left continue to rise until the wood reaches T > 200, so pyrolysis starts and because of the glowing combustion in the embers, at even higher temperatures the volatile gases can be ignited. Ignition is then not only a matter of the instantaneous heat flux than can penetrate the sample (where a critical heat flux value alone might be misleading) but also a function of the overall thermal penetration, which includes the time of exposure. Lower heat flux values for experiment 26 refer to higher temperatures in the sample. These experiments provide representative values for the ignition or no ignition situations. Data is also obtained from wood but the change in properties (especially conductivity) makes it harder to analyze the process.

Figure 3.19 shows the temperature profiles for the non-flaming experiment. Again, as shown for the vermiculite (exp_28), there is a fast increase in the heat flux until it reaches a maximum of approx. 8.2 kW/m$^2$. However, the temperatures in the sample are lower than 100 °C so there is no generation of volatile gases. Due to the consumption of the embers and the absence of wind, combustion stops and the heat transfer to the sample decreases. At some point, it is even possible to see negative values of heat flux. This is because the wood has a much higher thermal inertia than the light embers located on the surface. The embers cool down much faster and then at some point the temperature inside of the sample (see the slow cooling process on figure 3.19 left) is higher than the surface temperature and the heat flux is reversed.

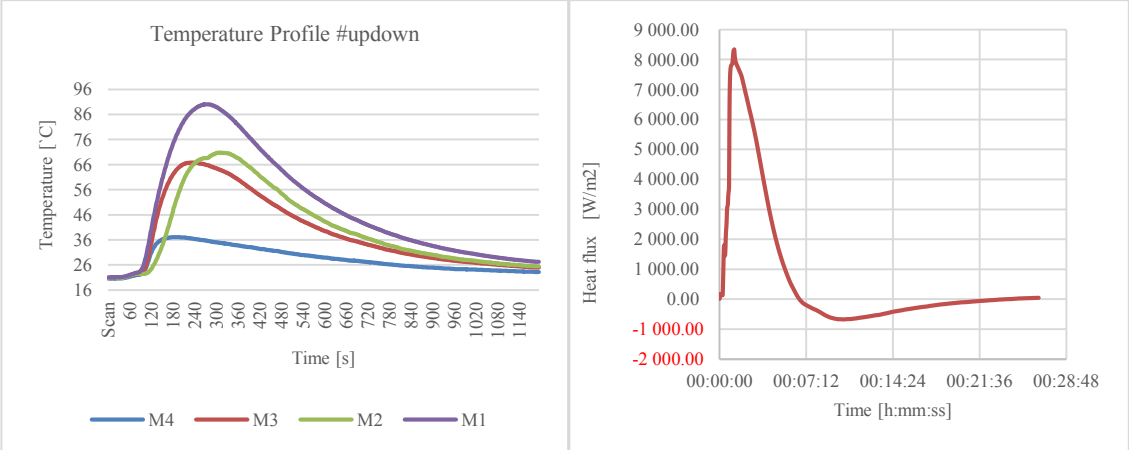


Figure 3.19. Experiments by Kamila Kempna. Experiment 24: Embers on redwood (40 gr). Left: Temperature profile. Right: Heat flux.

### 3.2.6 Limitations of the experiments

The limitations and some of the errors contained in the results provided above have been discussed for every section. A short summary is provided in the following paragraphs.

When addressing the large scale experiments for the ember collection, many factors have influenced the results. Different measuring techniques provided different accuracies. Thickness measurements are essential to determine the density of each particle and then provide conclusions on the possible state of burning of the landing particles. The thickness for bark slices collected in E2 was not measured.

In the case of the small scale experiments, thinner thermocouples could be used to avoid the effect of the large holes in the wood. Also, it is always assumed that the thermocouples in section 1 and section 2 (3, 6 and 9 mm) are in the same line, and that is why the temperature profiles are shown as thermal penetration trough the wood. This assumes that the isothermal surface is parallel to the surface of the sample. Although it is a logical assumption, with the use of thinner thermocouples, the horizontal distance (currently 10 mm) between them could be reduced.

The heater has a surface of 130 mm by 45 mm. This is not, however, the actual heating surface, as was already mentioned. This is a limitation because the design of the location for the thermocouples was done using the initial value. Some thermocouples are not used (A, B, D, E) and others are barely used (C, L), mostly because they were located too far. This also affects the assumption mentioned in the previous paragraph.

The analysis for the dependence of the conductivity on the grain direction had to be done in a qualitative manner by studying the temperature profiles trough the wood. The 2 dimensional problem would require better instrumentation and modelling of the situation.

C clamps made of steel were used to hold the heater in place during the experiments. It was not possible to ensure that the pressure at which the heater had been pressed against the surface of the wood was constant. This affects directly the boundary conditions in the sample.

# 4 CONCLUSIONS

For the embers collected, it was shown that the measuring technique to determine the area and the thickness of every particle has a profound effect on the validity of the analysis performed. Accurate measurements permit the determination of particle densities which in turn can help determine the likelihood of ignition and the burning rate according to fire characteristics.

The results compared very well to what was found on the experiments performed in 2013. Most of the particles are bark slices and, in lesser degrees, branches. Average mass and densities were calculated for the different types of particles. Fuel loading per meter square was highly dependent on the location of the ember plot, from 0.2 to 98 $gr/m^2$ (ground surface). It was assumed that all branches are perfect cylinders. Some small branches presented very high densities, which could indicate that they landed still flaming.

More embers were collected in ember plot 2 than in plots 1 and 3. The new measuring technique resulted in more particles being measured, but the difference is too big to be caused only by this factor. It was thought that higher winds or more intense fires may be the cause, but this was disproven since wind conditions are similar between E1and E2 and fire intensity is higher for E1. It is then believed that the location of the plots, the density of the vegetation, the involvement of the canopy fuels (not accounted for in the calculation of fire intensity) and other factors have a high influence on the collection of short-range embers.

With relation to the small scale experiments, four different sets of experiments were performed on wood. In two of the four sets the surface temperature was measured. For the first set of experiments, with non-insulated samples it was shown that the one dimensional, heat flux assumption is not valid. Isothermal lines in the sample are not parallel to the surface. It was also shown that the initial method for measuring the surface temperature had a big impact on the charring rate. The results from experiments 1-6 are not used for further comparisons.

In the second set of experiments (7-12) the samples were insulated. It is shown that this has a positive impact on the heat transfer phenomenon, since losses in the edge are reduced and the one dimensional approach used to calculate heat flux is valid. All the analysis are considered until the temperature in the sample reaches 300 °C, at which point charring occurs and heating by conduction is immediately affected.

It was seen for most of the experiments that when the heater supply is set to 120V, the temperature increase in the surface and in the inside of the sample is very rapid. Charring tends to occur in less than 5 minutes and glowing combustion occurred for both insulated and non-insulated samples. These results are always analyzed but the focus is always made on experiments set to 60V and 90V, since the thermocouple set up (3 mm, 6 mm and 9 mm from the surface) is deemed not ideal to study such an aggressive thermal attack on the sample.

The qualitative analysis on grain direction showed agreement with the literature. Temperatures reached at 50 mm from the edge were 100-150% higher for a heat flux parallel to the grain direction. The situation is recognized to be a two dimensional heat transfer problem. Values of heat flux are not calculated since it falls out of the scope of this report.

Experiments 19-25 studied the effect of inert heating on an inert, homogeneous, isotropic material. 7 different voltage supply ratings were used. The influence of charring on the one dimensional assumption was shown, as well as the influence of losses in the edge. The contact between the heater and the sample and its relevance to the heat transfer process at the edge was also studied.

Heat flux was calculated for experiments at 60V and 90V. The conservative assumption that charring occurs when the surface temperature of the heater reaches 300 °C was made (assuming it equals the surface temperature of the sample). A constant conductivity is used and the limitations of this assumption are discussed. Values were compared to those derived from experiments with embers (pieces of bark) on redwood and vermiculite. It can be seen that the rate of heat flux can be more severe (but also shorter) when embers are used (as opposed to the electrical heater).

The limitations of the experimental procedures and the possible sources of error were discussed in each independent analysis. A summary of their impact and ways to reduce their effect was presented.

### Future work

Future work could be focused on incorporating to the analysis the determination of critical values of heat flux for ignition under different circumstances, taking into consideration the temperature dependent properties of the wood.

This analysis showed limitations in understanding the heat transfer process once charring has occurred. Several studies have been made in the past to analyze the way properties of wood change when samples are exposed to high temperatures; results from theses analysis could be applied to better quantify the critical heat flux on wood (e.g. determination of charring rate). Once this is done, the electrical heater could be used again to simulate these heat fluxes (a more powerful heater will have to be used). In this project the main idea was to study the impact of conduction in the wood and understand the possibilities for the use of the heater. Future studies could try to replicate with more accuracy the temperature profiles in the wood when it is exposed to hot embers.

Finally, two main limitations associated to the heater should be addressed: first, wind is not considered and it has been proven to be a critical factor for ignition and second, the study on single samples of wood does not account for the way the geometry affects the heat transfer (angles, joints, etc.).

# V. ACKNOWLEDGEMENTS

Most of the work done for the experiments with the heater was built upon the efforts of Kamila and Chris at designing and building the test table. Special thanks to Kamila with whom I shared the load of this project, to Chris and Eric for their help during these months and to Juan for his valuable insight.

To my supervisor, Prof. Simeoni, who managed to find the resources to include me in the large scale experiments performed at New Jersey in March of this year, and who provided guidance and counsel throughout the whole project.

# VI. REFERENCES

[1] Anthenien, R., Tse, S., Fernandez-Pello, C. “On the trajectories of embers initially elevated or lofted by small scale ground fire plumes”. Fire Safety Journal. 41, 349–363. 2006.

[2] Bilbao, R., Mastral, J., Aldea, M., Ceamanos, J., and Betrán, M. “Experimental and Theroretical Study of the Ignition and Smoldering of Wood Including Convective Effects”. Combustion and Flame Journal. 126:1363-1372. 2001.

[3] Cohen, J. “Preventing Disaster. Home Ignitability in the Wildland-Urban Interface”. Journal of Forestry. 15 – 20. 2000.

[4] Cohen, J. “Relating flame radiation to home ignition using modeling and experimental crown fires”. Canadian Journal of Forest Research. 34, 1616–1626. 2004.

[5] El Houssami, M., Mueller, E., Filkov, A., Thomas, J., Skowronski, N., Gallagher, M., Clark, K., Kremens, R., Simeoni, A. “Experimental Procedures Characterizing Firebrand Generation in Wildland Fires”. *Submitted to relevant journal.*

[6] Ellis, P. “The likelihood of ignition of dry-eucalypt forest litter by firebrands”. International Journal of Wildland Fire. 24, 225-235. 2015.

[7] Koo, E. “Firebrands and spotting ignition in large-scale fires”. International Journal Of Wildland Fire. 19, 818-843. 2010.

[8] Leikanger, K. “Material properties and external factors influencing the charring rate of solid wood and glue-laminated timber”. Fire and Materials. 35, 303-327. 2011.

[9] Manzello, S., Suzuki, S., Hayashi, Y. “Enabling the study of structure vulnerabilities to ignition from wind driven firebrand showers: A summary of experimental results”. Fire Safety Journal. 54, 181-196. 2012.

[10] Manzello, S., Cleary, T., Shields, J., Yang, J. “Ignition of mulch and grasses by firebrands in wildland-urban interface fires”. International Journal of Wildland Fire. 15, 427-431. 2006.

[11] Manzello, S., Park, S., Cleary, T. “Investigation on the ability of glowing firebrands deposited within crevices to ignite common building materials”. Fire Safety Journal. 44, 894-900. 2009.

[12] Mueller, E., Skowronski, N., Clark, K., Kremens, R., Gallagher, J., El Houssami, M., Filkov, A., Butler, B., Hom, J., Mell, W., Simeoni, A. "An Experimental Approach to the Evaluation of Prescribed Fire Behavior". *Submitted to relevant journal.*

[13] Sardoy, N. "Transport and combustion of Ponderosa Pine firebrands from isolated burning trees". First International Symposium on Environment Identities and Mediterranean Area. 6-11. 2006.

[14] Spearpoint, M. and Quintiere, J. "Predicting the Burning of Wood Using an Integral Model". Combustion and Flame. 123, 308-324. 2000.

[15] Spearpoint, M. and Quinitiere, J. "Predicting the piloted ignition of wood in the cone calorimeter using an integral model – effect of species, grain orientation and heat flux". Fire Safety Journal. 36, 391-415. 2001.

[16] Suleiman, B., Larfeldt, J., Leckner, B. and Gustavsson, M. "Thermal conductivity and diffusivity of wood". Wood Science and Technology. 33, 465 – 473. 1999.

[17] Stein, S., Comas, S., Menakis, J., Carr, M., Stewart, S., Cleveland, H., Bramwell, L. and Radeloff, V. "Wildfire,, Wildlands, and People: Understanding and Preparing for Wildfire in the Wildland-Urban Interface" USDA. General Technical Report RMRS-GTR-299. 2013.

[18] Viegas, D. "Recent Forest Fire Related Accidents in Europe". JRC Scientific and Technical Reports. EUR 24121 EN. 2009